Generation of Photocurrent from Photosystem I

Biomolecular Complexes

by

Rajay Kumar

Submitted to the Department of Electrical Engineering and Computer Science

in Partial Fulfillment of the Requirements for the Degrees of

Bachelor of Science in Electrical Science and Engineering

and Master of Engineering in Electrical Engineering and Computer Science

at the Massachusetts Institute of Technology

May 23, 2003

Author_____
Department of Electrical Engineering and Computer Science
May 23, 2003

Certified by_____
Marc A. Baldo
Thesis Supervisor

Accepted by_____
Arthur C. Smith
Chairman, Department Committee on Graduate Theses

Generation of Photocurrent from Photosystem I Biomolecular Complexes
by
Rajay Kumar

Submitted to the
Department of Electrical Engineering and Computer Science

May 23, 2003

In Partial Fulfillment of the Requirements for the Degrees of
Bachelor of Science in Electrical Science and Engineering
and Master of Engineering in Electrical Engineering and Computer Science

ABSTRACT

Photosynthetic proteins are used in organic devices to generate photocurrent. A setup consisting of a monochromator and lock-in amplifiers is used to measure the photocurrent along with an HP4156 analyzer. Atomic force microscopy images are also taken including those taken with a voltage-biased tip. Some devices are shown to work initially under illumination and then fail upon subsequent illumination. A charge trapping mechanism is postulated to cause the failure. Nonetheless, the devices hold enormous potential and the preliminary results show that research in this area will be fruitful, even though evaporation of protective layers does not usually yield functional devices.

Thesis Supervisor: Marc A. Baldo
Title: Assistant Professor, Dept. of Electrical Engineering and Computer Science

Table of Contents

Acknowledgements

I would like to thank first and foremost Prof. Marc Baldo for his kind generosity and support from day one. This project would be nothing without his guidance and wisdom.

I would also like to thank my lab partner, Julie Norville. Her dedication and perseverance helped make this project the success it has been.

My family deserves much love and thanks. Without their support and love, I would be finishing much more grumpier if at all!

Paul, Jon, and Andrew: without you guys there for me at the apartment, I imagine I'd be much more homesick. I'm really going to miss you guys.

Brian Chan: Thanks for always being there for me whenever research got me down. You don't realize how much it has eased my mind talking to you sometimes.

My other labmates: Michael, Rupa, and Benjie: it has been a lot of fun working with all of you over the past year. There won't be another group like you all – I mean that in a good way, of course. Thanks especially to you, Michael, for showing me the ropes and being there to talk to.

Thanks Patrick Kiley for helping with the very biological aspects of this project. You really know your stuff well and have been very helpful. Best of luck in the future!

A special thanks is due to the Lord Foundation which provided summer UROP funding for part of my research.

List of Figures

List of Equations

List of Tables

I. Motivation

The long-sought goal of molecular scale device complexity is something which has just started to come into focus for scientists and engineers. However, such structures already exist in nature. Through eons of evolution, protein structures have been used to fill a variety of tasks including cellular locomotion, enzyme catalysis, and generation of photocurrent. Proteins like Photosystem I (PSI) and reaction centers of the bacteria *Rhodobacter Sphaeroides* are able to absorb light at certain wavelengths and break apart excitons into charges, generating current. These proteins and their variants have existed in nature as part of chemical pathways for plant respiration since early forms of life first existed. In spite of this, the current they produce has not been used for any other means. Thus, incorporating the protein into electronic devices will show that this naturally occurring complexity can be harnessed for human use. Furthermore, using this particular protein will show the feasibility of creating a protein photovoltaic which has the potential to be more efficient than current solar cells, opening new doors in device engineering.

The need for highly efficient solar cells comes from a historical dependence on combustible materials, such as coal and oil. As a result, the world's natural oil deposits are running dry and the pollution caused by the combustion of these sources has negatively impacted the environment. To this end, alternate sources of energy have been researched, including wind power, tidal power, and solar power. A leading candidate among these for a sustainable source of alternate energy is solar power (EIA, 2001). However, energy generated by conventional photovoltaic devices remains too expensive due to excessive fixed costs such as the cost of photovoltaic devices themselves. There is much hope, however, if one looks toward nature. Highly efficient photovoltaic processes

occur every day in all plants and bacteria which perform photosynthesis. Through the use of complicated proteins, plants are able to generate current from incident light. Harnessing such mechanisms could mean an inexpensive renewable source of energy for the future.

In addition, PSI and other photosynthetic complexes have properties not found in conventional silicon technology. For example, the complexes employ molecular electronic circuits to separate charge, allowing them to operate at frequencies as high as one terahertz. They also make excellent photodetectors since they do not require an applied bias and are expected to possess very large internal resistance. Consequently, photosynthetic complexes may find applications in low noise photodetectors. Such efficiency will allow for extremely sensitive photodetecting equipment.

Furthermore, electrical integration of proteins has never before been accomplished. Incorporating such structures into devices will show that protein-based electronics are feasible. Such electronics will give engineers the opportunity to make use of the precise systems found in biology, opening a new era in device complexity. Traditional lithography techniques cannot achieve the precise assembly exhibited by the chemical machinery found in proteins.

Using photosynthetic complexes in photovoltaic applications may have additional advantages as compared to silicon photovoltaics. Due to the brittle nature of silicon, it is not easily used in fabric materials. However, photosynthetic complexes can be self-assembled onto a variety of substrates, including flexible ones such as fabrics, paving the way for pervasive wearable computing and smart fabrics.

Furthermore, this research can lead to photovoltaics that are less harmful to the environment. Even though today's solar cells create pollution-free energy, processing the silicon takes its toll on the environment. In this work, the active electronic components are extracted from spinach and other natural sources.

In the following pages, the background, methodology, and results of experiments determining the feasibility of electrically integrating photosynthetic proteins will be discussed. In the background section, the protein's structure and function will be elaborated upon in further detail. Additionally, a summary of previous related work will be given. Next, the steps used to create the devices from its constituent materials will be discussed. This encompasses the self-assembly procedures used to bind the protein to a substrate as well as the procedures for the application of protective layers. Following this, the setups used to measure the devices and the results from these measurements will be discussed. One setup measures the generated photocurrent versus the wavelength of exciting light and another setup measures the current versus the voltage applied of the devices. The results section will explain the significance of the data in regard to electrical integration of the protein. Finally, the significance of this work and future work will be discussed in the conclusion.

II. Background

A. Protein Background

i. Proteins in Nature

The proteins used in this research are found in nature in plant cells. Cells are the building blocks of almost all living things and come in many different varieties. Each cell is powered by energy derived from other living creatures, as is the case with most animals, by energy from the sun, as is the case with most plants and some bacteria, and/or by other exotic sources of energy, such as thermal energy, as is the case for some organisms dwelling at great ocean depths and thermophilic bacteria. For the vast majority of all living things on this planet, energy ultimately comes from the sun. The organisms that directly obtain energy from the sun do so through a process called photosynthesis.

Within each cell are particular components called organelles. These organelles each perform specific tasks to help keep the cell and the organism it may be a part of functioning. Within green plant cells and some bacteria are organelles called chloroplasts. These organelles are membrane-bound and serve to obtain energy from incident light. Within the chloroplasts are stacks of plate-like structures called grana. The plate-like structures are called thylakoids. It is within the membranes of these thylakoids where the photosynthetic proteins reside. These thylakoids are actually thin sacs containing a solution called a lumen. The lumen is filled with protons, making it more acidic than the outside, known as the stroma. The lumen and stroma play crucial roles for proteins in the thylakoid membrane, where photosynthesis occurs (Figure 1). (Purves, *et al.*, 1995)

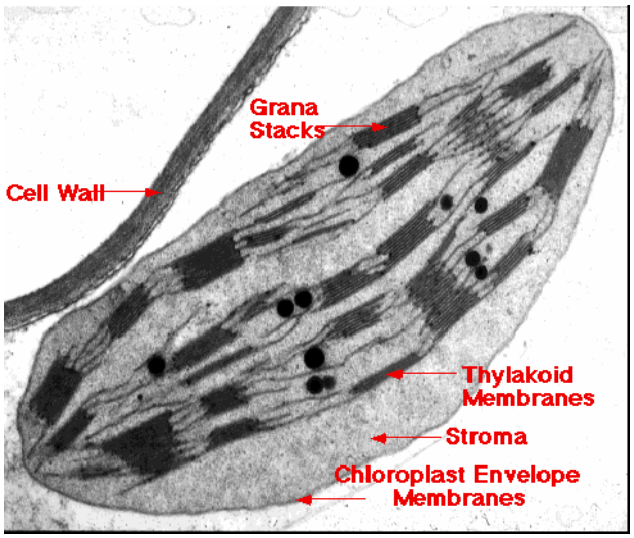

Figure 1: Transmission electron microscopy image of a chloroplast inside a plant cell. The stroma can be seen in the majority of the chloroplast, whereas the lumen is only inside the tightly-packed thylakoids. (http://www.blc.arizona.edu/courses/181gh/rick/photosynthesis/chloroplasts.html)

Photosynthesis is the chemical reaction where carbon dioxide and water are the reactants and sugar, oxygen, and water are the products. This chemical reaction does not occur in one step; instead, many small reactions occur in order to reach the final product. These reactions can be divided into two groups: reactions used to produce adenosine triphosphate (ATP) and reactions that use ATP to produce sugar. Light is used in the pathway to produce ATP, known as photophosphorylation. (Purves, *et al.*, 1995)

Reactions in this pathway are catalyzed by enzymes called photosystems. These photosystems contain pigments which absorb light of specific wavelengths, taking them from the ground state to the excited state. In the excited state, the pigments have more energy and are able to transfer this energy to other chemicals. The pigments chlorophyll *a* and chlorophyll *b* are the most abundant in green plants. Both of these molecules contain a ring structure with a magnesium ion in the middle. A hydrocarbon chain forms a "tail" on each pigment. (Purves, *et al.*, 1995)

Within the photosystems, pigments transfer energy to other molecules. This occurs after a pigment is excited by light and then donates an excited electron to an

accepting molecule known as an oxidizing agent. This name is given due to the fact that it assists in the pigment's oxidation, or loss of an electron. (Purves, *et al.*, 1995)

Photophosphorylation occurs in two different varieties: cyclic and noncyclic. In noncyclic photophosphorylation, a product called $NADPH + H^+$ is produced along with ATP and some O_2. $NADPH + H^+$ and ATP are both reducing agents, that is, they both donate electrons to other molecules. To create $NADPH + H^+$, a reducing agent strong enough to reduce $NADP^+$ to $NADPH + H^+$ is created. This reducing agent is created by photosystem I (PSI), a thylakoid membrane-bound protein surrounded by many chlorophyll molecules, which act like antennas for light. PSI has a reaction center containing a chlorophyll *a* molecule known as P_{700} due to the fact that it maximally absorbs light with a wavelength of 700nm. Another protein, photosystem II (PSII) also contains many chlorophylls, but it takes electrons from water and passes them to a chain of electron carriers which eventually create ATP from adenosine diphosphate (ADP) and inorganic phosphate (PO_4^{3-} or P_i). PSII also contains a chlorophyll *a* in its reaction center, but it is known as P_{680} because it absorbs maximally at 680nm. Noncyclic photophosphorylation begins when PSII absorbs photons, sending electrons from P_{680} to an oxidizing agent known as pheophytin-I and thereby oxidizing P_{680} to P_{680}^+. (Purves, *et al.*, 1995) P_{680}^+ is reduced back to P_{680} by electrons obtained from the oxidation of water into H^+ and O_2. The electron passed to the oxidizing agent is passed to other electron carriers, eventually finding its way to PSI via a carrier known as plastocyanin. In this chain, energy is lost each time the electron is passed. This energy is used to convert ADP and P_i to ATP. In PSI, P_{700} becomes excited after absorbing photons and donates an electron to an oxidizing agent known as ferredoxin, becoming oxidized to P_{700}^+.

Electrons passed via plastocyanin reduce P_{700}^{+} to P_{700}. Now, two protons (H^{+}) from the original oxidation of water and two electrons from ferredoxin reduce $NADP^{+}$ to NADPH + H^{+}, the final product (Figure 2). (Purves, *et al.*, 1995)

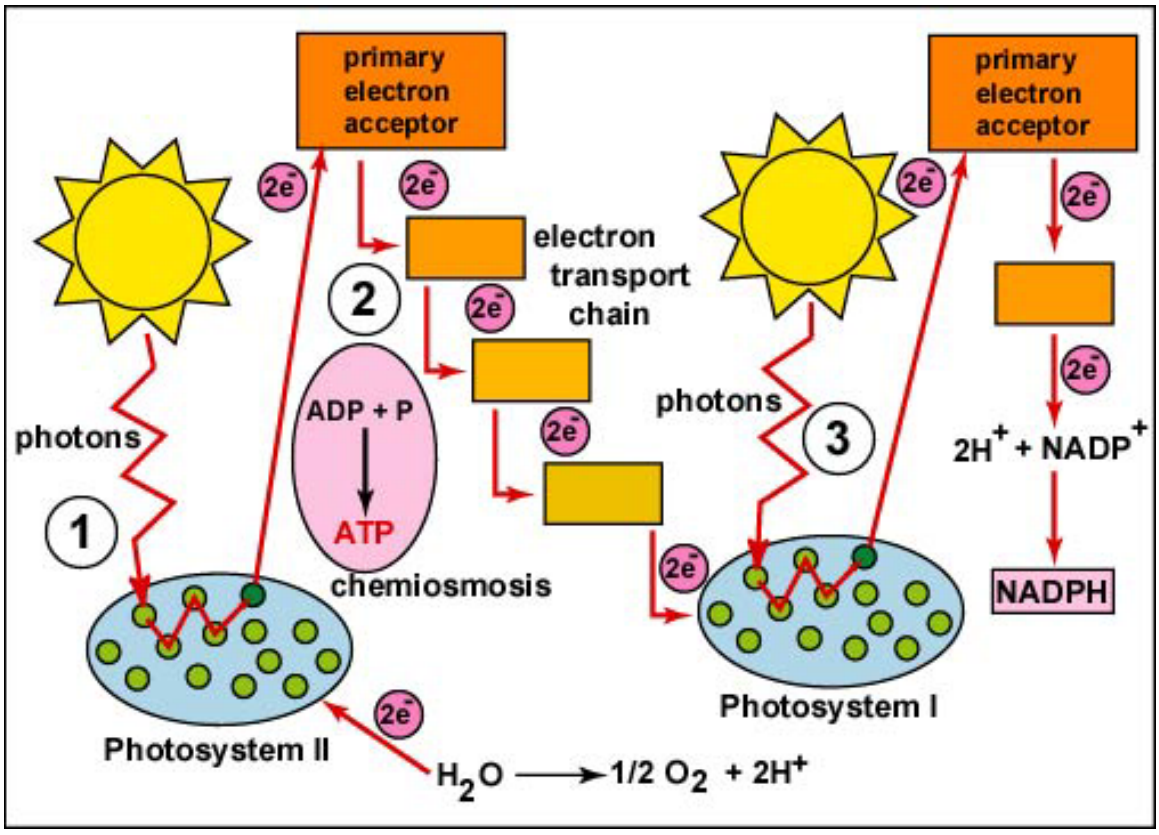

Figure 2: Noncyclic photophosphorylation. Note the creation of NADPH + H^{+} and the hydrolysis of water involved. (http://www.cat.cc.md.us/courses/bio141/lecguide/unit1/eustruct/phofig2.html)

The other form of photophosphorylation, cyclic photophosphorylation, only produces ATP as its final product. This pathway begins when P_{700} in PSI's reaction center becomes excited after absorbing a photon. The excited P_{700} then donates an electron and reduces oxidized ferredoxin. The reduced ferredoxin passes its electron to plastoquinone (PQ), another oxidizing agent. The reduced PQ then passes the electron to a cytochrome complex (Cyt). The electron is then passed one last time to plastocyanin, which donates the electron back to PSI, thus completing the cycle. The energy lost via

the carriers is used to convert ADP + P_i to ATP. The cycle is maintained by energy from light which is ultimately used to create ATP (Figure 3). (Purves, *et al.*, 1995)

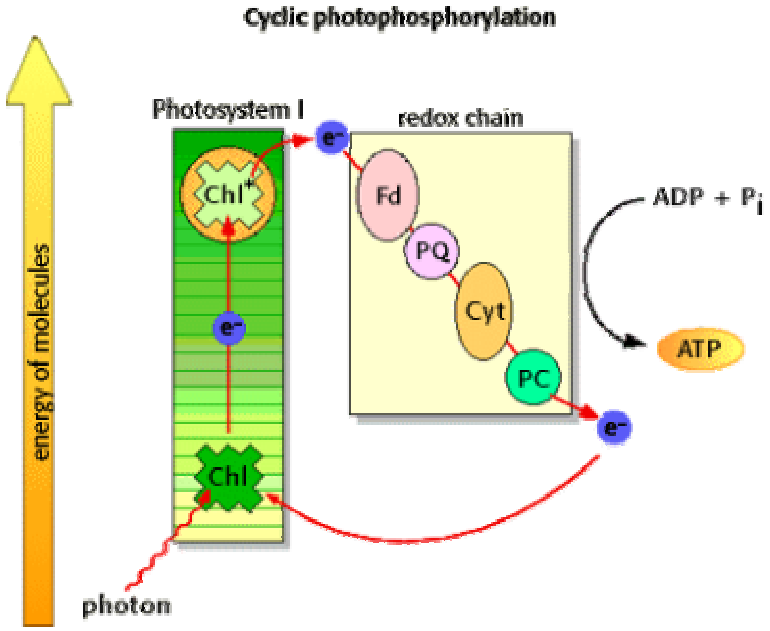

Figure 3: Cyclic photophosphorylation. Note that only ATP is created in this process. (http://www.biology.arizona.edu/biochemistry/problem_sets/photosynthesis_1/07t.html)

In the second pathway, carbon dioxide is used to create glucose, a sugar. In a process called the Calvin-Benson cycle, carbon dioxide combines with other molecules and forms glucose. Using the energy gained from ATP and NADPH + H^+ during each cycle, a molecule of glucose is made after six cycles. The resulting ADP + P_i and $NADP^+$ from each cycle are re-energized to form ATP and NADPH + H^+ via the photophosphorylation pathways (Figure 4). (Purves, *et al.*, 1995)

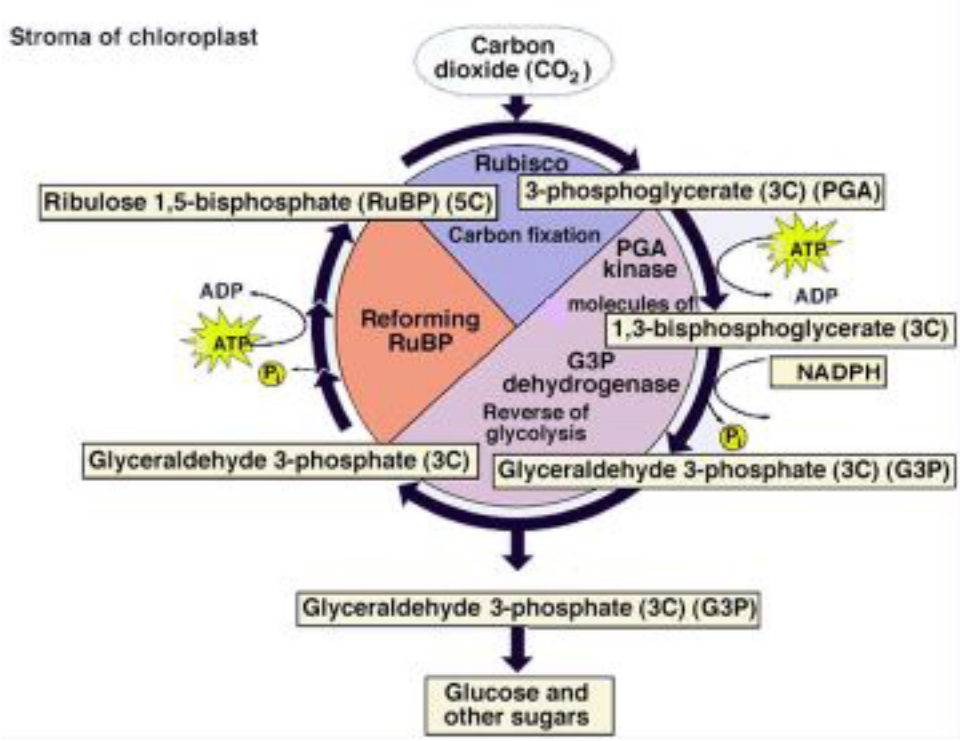

Figure 4: Calvin-Benson cycle. Note the use of ATP and NADPH + H^+ to create sugars. (http://scidiv.bcc.ctc.edu/rkr/Biology201/lectures/Photosynthesis/Photosynthesis.html)

ii. Protein Structure and Function

A protein is a chain of amino acid subunits found in all biological organisms. The polymer chain consists of carbon-nitrogen bonds, where one end of the protein has a nitrogen atom (the N-terminus) and the other end has a carbon atom (the C-terminus). Most proteins are enzymes, or catalysts for specific chemical reactions. Photosystem I, or PSI, is one such protein that is able to use the energy from light to break an exciton apart into a positive and negative charge in order to harness the energy from light. A computer simulated model of PSI can be seen in Figure 5 and in Figure 6. The carbon-nitrogen bonds are represented by tubes of various colors. The chlorophyll molecules surrounding the protein form an antenna complex can be seen as magnesium ions surrounded by a molecular ring.

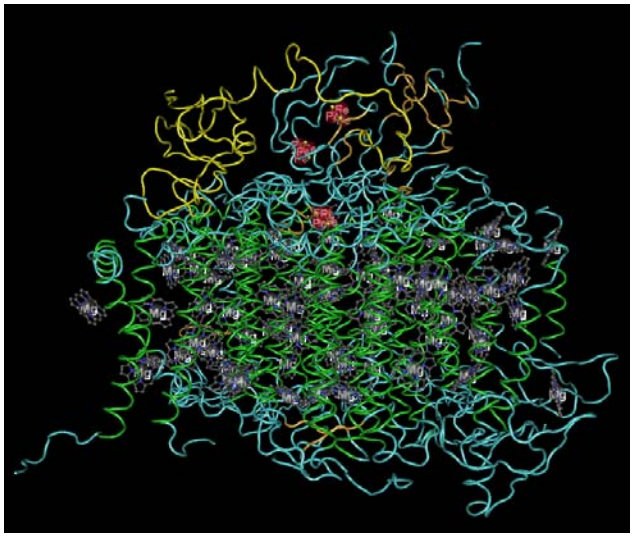

Figure 5: View of PSI from the side. The red clusters are Fe_4S_4 clusters. The gray clusters are the Mg atoms in the chlorophyll molecules. The rest are part of the protein backbone, giving the PSI its structure. Attention should be drawn toward the green α-helices which give PSI its discoidal shape and the grey magnesium atoms in the centers of the chlorophyll molecules. (NCBI MMDB)

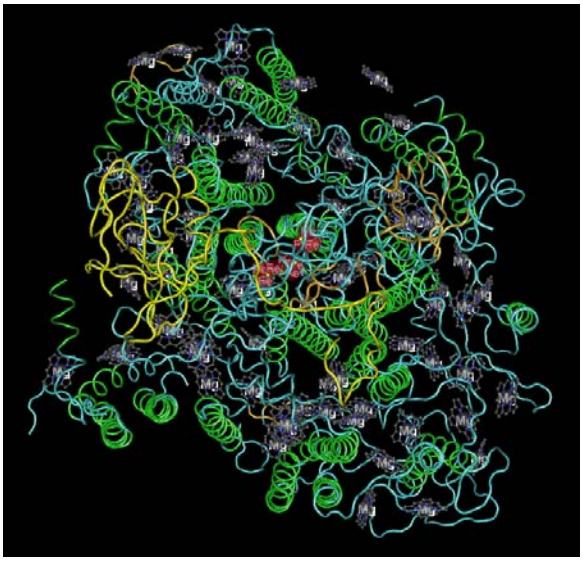

Figure 6: View of PSI from the top. The Fe_4S_4 clusters can be clearly seen on the central axis of the protein. Also, the radial arrangement of the chlorophylls is readily seen. (NCBI MMDB)

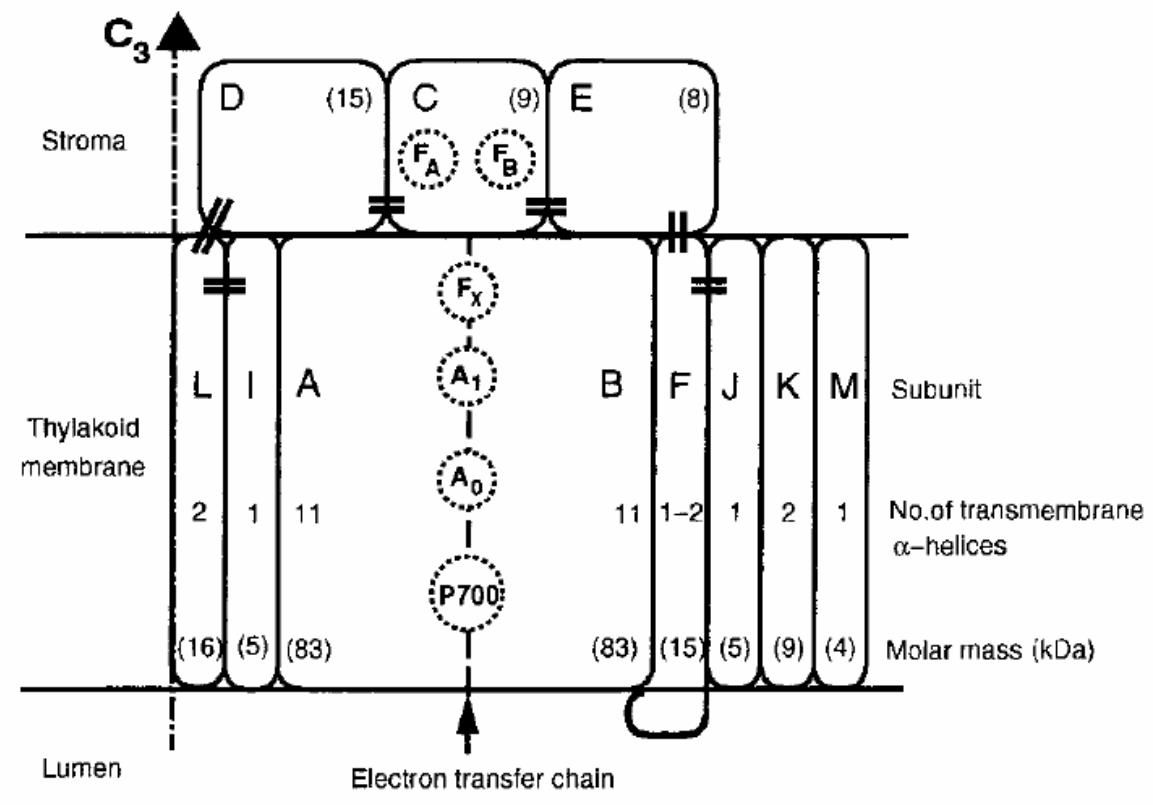

Figure 7: The subunits of cyanobacterial PSI. Subunits are indicated by the unique letters in their names, i.e. A denotes PsaA. Under the letters are listed the numbers of transmembrane α-helices in the subunit. Cofactors such as F_A and F_B and P_{700} are shown in dotted circles. (Schubert, et al., 1997)

Photosystem I has embedded within itself molecules used as antennas for capturing the light of solar energy and it also contains molecules used as electron donors as shown in between the PsaA and PsaB subunits in Figure 7. In the previous description of photosynthesis, it was explained that P_{700} becomes excited and passes an electron to ferredoxin. In reality, this occurs, but the electron is passed from P_{700} to other cofactors before reaching ferredoxin. P_{700} acts as a primary electron donor and resides in the reaction center (RC), as illustrated in the description of photosynthesis. The P_{700} becomes excited after absorbing a photon, creating a directed transmembrane charge separation. The charge separation is able to travel across the membrane since the reaction core spans the thylakoid membrane from the inner (lumenal) hydrophilic end,

through the hydrophobic central portion and to the outer hydrophilic (stromal) end. After P_{700} becomes excited, the primary electron acceptor, A_0 (the primary electron acceptor, assumed to be a chlorophyll *a* monomer), gains an electron, creating the ionic pair $P_{700}^{+}A_0^{-}$ within 2 to 4ps. A_0^{-} then gives its electron to A_1 (a secondary electron acceptor in the form of a phylloquinone molecule) within 20 to 50 ps, reducing it to A_1^{-}. Now P_{700}^{+} and A_1^{-} form a semi-stable pair. Next, the Fe_4S_4 cluster, F_X, is reduced within 200ns. Then either F_A or F_B are reduced by F_X (the actual route of the electron remains unclear) in less than 500 ns. The Fe_4S_4 clusters F_A and F_B are in the subunit PsaC where they reduce ferredoxin within 500ns to 100μs. The original electron donor, P_{700}^{+}, is then reduced by the copper-containing protein plastocyanin within 10 to 100μs. This is the process by which PSI transfers the energy of an incident photon into an electron during photosynthesis. (Schubert, *et al.,* 1997)

PSI varies in structure in the organisms in which it is found. Though there are various forms of PSI, the basic structure and functionality of the protein remains relatively constant. For example, cyanobacterial PSI consists of 11 subunits called PsaA to PsaF and PsaI to PsaM whereas plant PSI lacks PsaM but have subuits PsaH, PsaG, and PsaN. The subunits of cyanobacterial PSI are shown in Figure 7. The subunits PsaA and PsaB surround the reaction center and bind to nearly 100 chlorophyll *a* (Chl*a*) molecules of the core antenna system as well as F_X, the Fe_4S_4 cluster. PsaC contains the two Fe_4S_4 clusters known as F_A and F_B. Cyanobacterial PSI is observed in trimers in crystals but such structures have not yet been found *in vivo* in plant PSI. (Schubert, *et al.,* 1997).

As evidenced by the computer rendered pictures of PSI in Figure 5 and Figure 6, PSI contains many α-helices, as shown in green. These form the core structure of the protein and help keep it firmly in place within the membrane's phospholipid bilayer, a structure that is hydrophilic on its two surfaces and hydrophobic in the middle. These provide horizontal stabilization between the inner protein core and the outer subunits. Furthermore, 89 Chl*a* have been identified. When in the form of a trimer, PSI has a height of about 90Å and a radius of 105Å at the largest bulge, meaning each individual PSI has a diameter of about 105Å. The lumenal surface of the protein is relatively flat whereas the side facing the thylakoid exterior, or stroma, contains a ridge extending about 30Å above the surface of the membrane-intrinsic subunits (Figure 8). (Schubert, *et al.,* 1997)

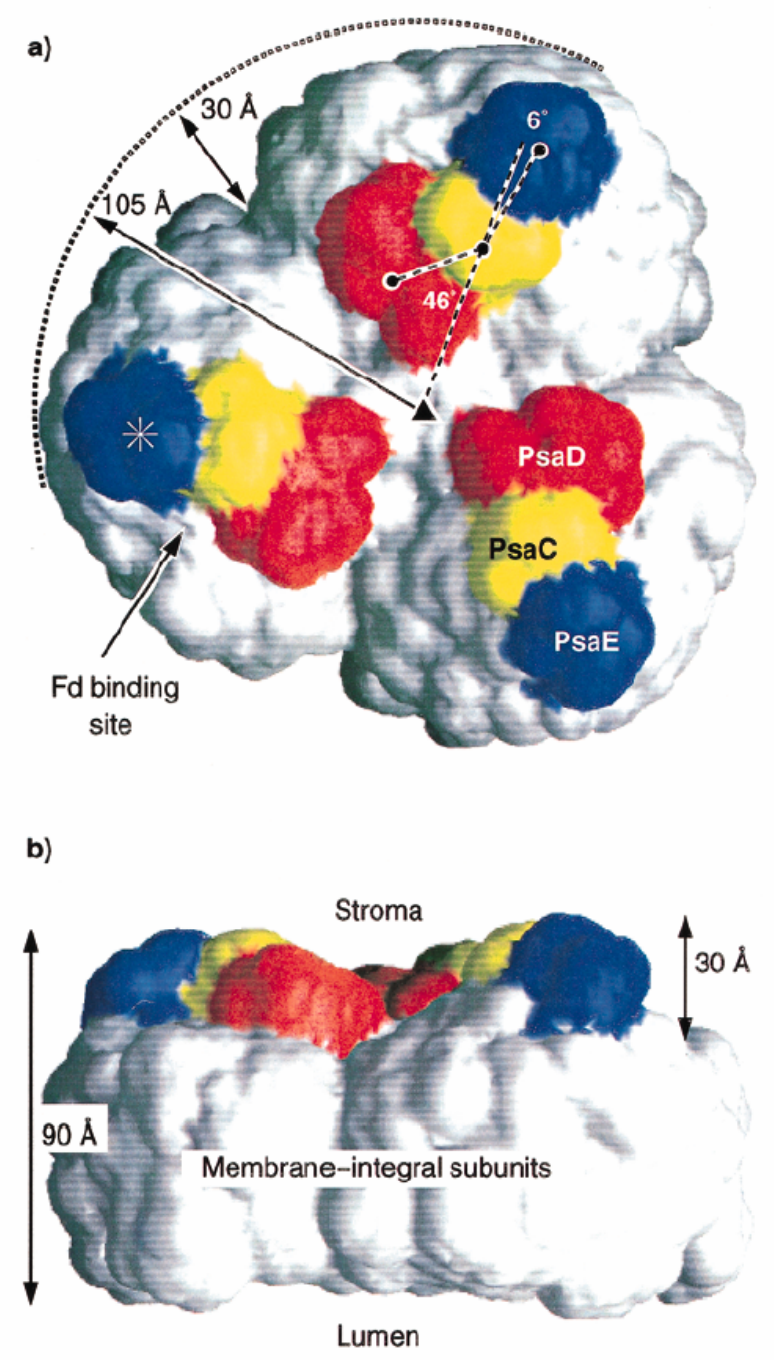

Figure 8: (a) Stromal view of PSI trimer. PsaC is shown in yellow, PsaD is shown in red, and PsaE is shown in blue. (b) View from the membrane plane. (Schubert, *et al.*, 1997)

PSI has about 30 α-helices in PsaA and PsaB out of a total of 43 α-helices. These create a central region where the cofactors of the electron transfer chain can be found. This includes P700 (a Chl*a* dimer), A_0, A_1, and F_X. Ten α-helices form a scaffold that

holds the cofactors of the electron transfer system while simultaneously enclosing and separating these highly reactive molecules from the surrounding antenna Chl*a*. (Schubert, *et al.,* 1997) In particular, stromal extensions of two α-helices point toward F_X, holding this Fe_4S_4 cluster in place. Cysteine, a sulfur containing amino acid capable of forming strong bonds to non-amino acid compounds, is found in two places in PsaA and in PsaB in cyanobacteria as well as higher plants. They help coordinate the F_X cluster by forming strong iron-sulfur bonds (Figure 9). (Schubert, *et al.,* 1997)

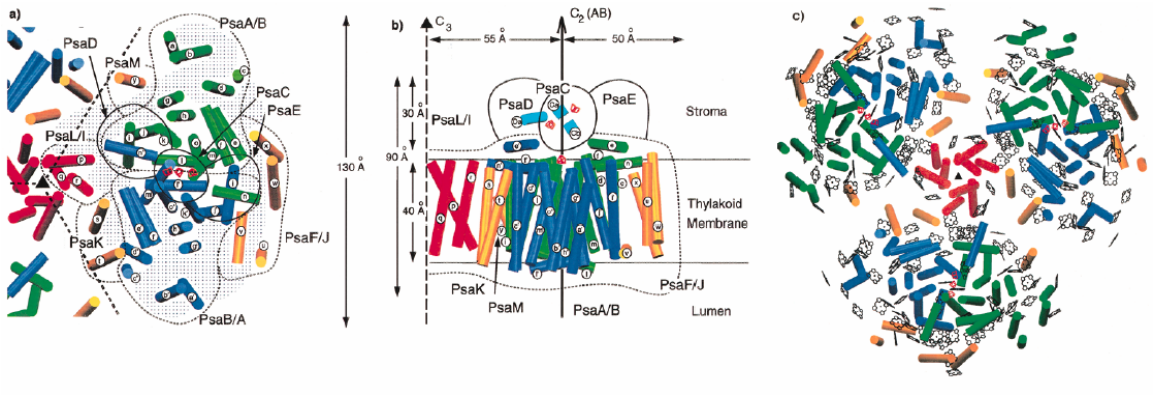

Figure 9: Arrangement of α-helices in PSI for (a) a lone PSI, (b) membrane-plane view, and (c) trimer view. (Schubert, *et al.*, 1997)

The subunits of PSI play crucial roles in the function and structure of the protein. PsaA and PsaB serve to bind electron donor molecules such as plastocyanin and/or cytochrome c_6 which reduce $P700^+$. PsaL is associated with trimer formation in cyanobacterial PSI. PsaF acts as a medium for the electron transfer between plastocyanin and $P700^+$. The α-helices of the subunits PsaL, I, K, J, F and M form a ring of α-helices around the core antenna system, indicating a primarily structural role. So, losing any subunit, particularly PsaF, PsaK, and PsaL, could partially disrupt the antenna system. PsaC is an extrinsic stromal subunit that binds to the terminal iron-sulfur clusters, F_A and F_B. Subunits PsaC, D, and E are extrinsic and stromal and can be easily removed by chaotropic agents, or agents that disrupt the hydrogen bonds formed when the protein is

in water, suggesting they are not strongly bound. PsaD contains a single α-helix that is found on the interface between PsaC and the membrane-embedded part of PSI. PsaC is only functional when PsaD is present. (Schubert, *et al.,* 1997). It has also been shown that PsaD partly covers PsaC stromally in a clasplike manner and interacts with PsaE. These three subunits form a cavity which serves as a docking site for ferredoxin. This cavity is a local binding minimum for ferredoxin which has an energy of interaction that is at least several multiples of k_BT (i.e. Boltzmann's constant multiplied by the temperature). (Lee, *et al.*, 2000)

Other chlorophyll besides the ones found in the reaction center play a crucial role in PSI. Particularly, the core antenna system of PSI is composed of almost 100 Chl*a*. This is complemented by other light harvesting structures such as membrane-attached phycobilisomes in cyanobacteria and light harvesting complexes I and II. The antenna Chl*a* take up a space which looks like a hollow elliptical cylinder that laterally surrounds the reaction center. It has a higher density of Chl*a* on the stromal side which makes sense as this faces toward the outside of the thylakoid membrane in which it is embedded. The Chl*a* are bounded by the ten innermost α-helices in the center of PSI that surround the reaction center's cofactors. Accessory Chl*a* and A_0 are believed to bridge the bulk antenna system with P700 in excitation energy transfer, implying that these accessory Chl*a* and A_0 play a dual role in that they also transport electrons in the opposite direction. (Schubert, *et al.,* 1997)

B. Previous Work

Though little prior protein photovoltaic research has been performed, there has been a great deal of research done with regard to the protein itself and its close relatives as well as with organic photovoltaics and photodetectors.

One relevant experiment performed prior involved a light-transducing protein called bacteriorhodopsin (BR). This protein naturally occurs in the purple membrane of the microorganism *Halobacterium salinarium* among others. BR naturally acts as a light-driven proton pump for an energy-balancing mechanism wherein a proton gradient is created across the cell membrane. It was discovered that BR retains its light-dependent properties when isolated and incorporated into an artificial membrane or thin polymer film. When enclosed between two electrodes, BR generates a temporal voltage when illuminated which is due to a pH sensitive electrode, i.e. this is not a photovoltaic effect. (Robertson, *et al.*, 1995) Coming from a charge displacement within BR, this photovoltage appears as a spike which quickly reaches saturation and then exponentially decays toward zero. The spike's amplitude is proportional to

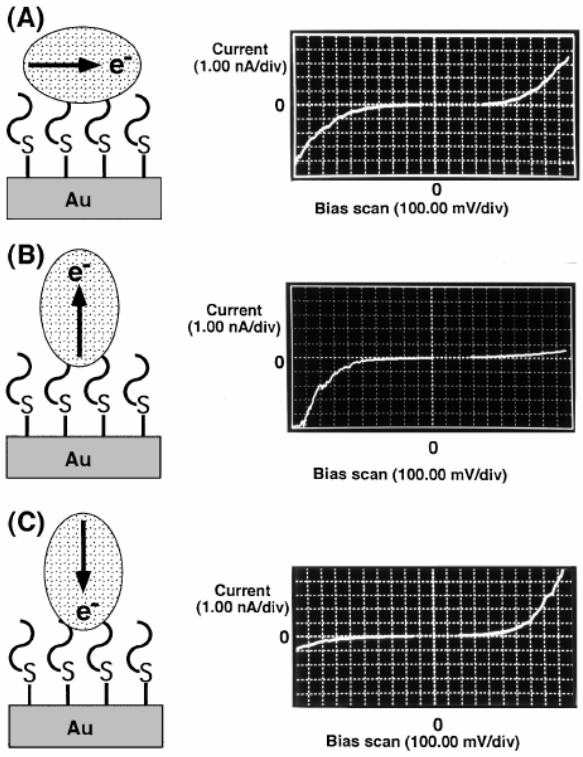

Figure 10: The orientation of PSI can be determined by the *I-V* curve. (A) When PSI is oriented parallel to the substrate surface, a semiconductorlike *I-V* curve can be observed. (B) and (C) A diodelike *I-V* curve is observed for PSI oriented perpendicular to the substrate surface. The size of the reaction center is enlarged. (Lee, *et al.*, 1997).

intensity and spectral distribution of the incident light pulse. The BR has also been prepared in polyvinylalcohol (PVA) films. (Frydrych, *et al.*, 2001). This shows that isolating PSI/RC-like proteins is possible and that a photovoltage has been obtained. However, this data does not indicate whether or not BR is useful for generating energy, since the only current generated is a displacement current.

Vectorial arrays of PSI have been prepared on substrates and different electrical properties arise from different orientations. However, without proper chemical treatment, the arrays consist of PSI, where each complex is oriented in a different direction, resulting in roughly zero net current flow when a voltage is applied and photocurrent is generated. It has been shown that if PSI has its electron transport vector parallel to the electrode surface, a semiconductor-like *I-V* curve with a ~1.8 eV band gap results. This band gap corresponds to the first excited singlet state of chlorophyll. However, when the PSI was oriented perpendicular to the substrate, the curve was more diode-like (Figure 10). Different orientations were obtained by different treatments of the gold substrate surface. Three different chemical treatments to create a negative, positive, or hydrophilic surface were used: mercaptoacetic acid ($HSCH_2COOH$), 2-dimethylaminoethanethiol [$(CH_3)_2NCH_2CH_2SH$], and 2-mercaptoethanol ($HSCH_2CH_2OH$). The results of the orientations are shown in Table 1. (Lee, *et al.*, 1997) Photovoltages have also been measured from single PSI bound to atomically flat gold via 2-mercaptoethanol. It was observed that a light-induced PSI electric potential reversal from positive to negative voltage occurs upon illumination. Under illumination, the electric potential on the reducing side of PSI develops a negative voltage following electron capture, whereas the potential is positive while in the dark. The average potentials of PSI in the dark are

0.77±0.14 V in one extremity of the reaction center, 0.62±0.08 V in the center, and 0.99±0.20 V in the other extremity. In the light, the average potentials are -0.47±0.26 V in one extremity, -0.41±0.24 V in the center, and -0.59±0.24 V in the center, and -0.59±0.26 in the other extremity of the PSI. Note this data was recorded with a Kelvin force microscopy tip that was significantly larger than a single PSI complex. Additionally, the effects of the feedback laser in this measurement are neglected, implying that there is indeed some light present in "dark" scans. The higher standard deviations of values taken in the light are most likely due to the variance of electron-hole recombination following photon absorption. The electrons return to $P700^+$ by recombination with iron-sulfide complexes and interaction with electrons from the gold substrate. (Lee, *et al.*, 2000).

Surface treatment of gold	Up (%)	Parallel (%)	Down (%)
Mercaptoacetic Acid	9.0	83.1	7.9
2-Dimethylaminoethanethiol	31.2	32.7	36.1
2-Mercaptoethanol	70.1	28.4	1.5

Table 1: Orientations of PSI on various derivatized gold surfaces. (Lee, *et al.*, 1997).

Another approach to orienting PSI and bacterial reaction centers (RCs), a more primitive photosynthetic protein, is through the use of bifunctional reagents. Bacterial RCs have been attached to the electrode surface via quinone derivatives which covalently immobilize the RC but still mediate electron transfer. Ubiquinone-10, a diffusionally mobile solubilized electron transfer mediator was also used to increase electron transfer efficiency. The limiting step of the electron transfer process is assumed to be the transfer from the immobilized mediator to the redox-active sites of the RCs because of the large distance between them. Orienting the protein minimizes the distance between the enzyme redox site and the electrode surface. The bifunctional reagents immobilize

proteins via functional groups of amino acids by either bonding with amino groups or thiol groups, commonly found on cysteine amino acids (Figure 11). The reagents consist of a condensed aromatic anchor group (a pyrenyl group) and a functional group and were bonded to a pyrolytic graphite electrode. It was shown that RCs whose sulfur-containing cysteine residue is blocked, making it unable to bind to the thiol treated electrode. A small photocurrent was observed when the RCs were bound to the amino treated electrode. This photocurrent was increased dramatically when solubilized ubiquinone-10 was added as an additional diffusionally mobile electron transfer mediator. But, immobilizing the RCs on the thiol-treated electrode gave the highest photocurrent without the solubilized mediator. An action spectrum showing current vs. wavelength for the RCs immobilized on the thiol-treated electrode is very similar to the action spectrum for native RCs (Figure 12). This implies that the RCs are in their native state while immobilized on the electrode. Since the solubilized ubiquinone-10 had little effect on the photocurrent for the RCs on the thiol-treated substrate, as the RC redox sites were oriented toward the electrode. The quantum efficiency of photocurrent formation was determined to be 100%. This very high quantum efficiency most likely results in the oriented immobilization of RCs, providing extremely efficient electron transfer from the RCs to the immobilized electron transfer mediator. (Katz, 1993)

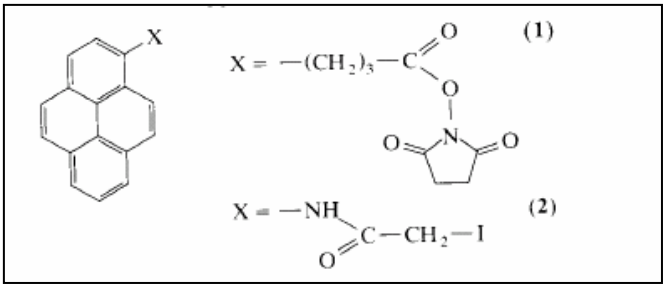

Figure 11: Bifunctional reagents - (1) (*N*-hydroxy-succinimidyl ester) is able to bond with amino groups and (2) (iodoacetoamidyl) is able to bond with thiol groups, commonly. (Katz, 1993)

It has also been previously shown by Minai, *et al.* that the PsaD subunit assembles into PSI via an exchange mechanism. PsaD has previously been shown to assemble into thylakoids spontaneously, specifically into the PSI complex. Studies also show that new PsaD subunits replace the in situ present PSI by an exchange mechanism. This was done by using recombinant PsaD in conjunction with native PsaD. The recombinant PsaD differed from the native PsaD in that it has a six-histidine tag at one terminus of its amino acid sequence. It was determined that on average, about half of the native PsaD population was replaced by recombinant PsaD by subtracting the amount of free protein that reacted with the anti-His antibodies, indicating recombinant PsaD, from the amount of free protein that reacted with the anti-PsaD antibodies, which reacted with both native and recombinant PsaD. It was also determined that the ratio of recombinant PsaD in the general PsaD population equaled its ratio in the PSI-assembled PsaD population, indicating that native and recombinant PsaD had the same affinity for PSI. It was further ensured that the histidine tag did not force the native PsaD to leave PSI and that the exchange mechanism is general enough to work in two different types of PSI. Furthermore, the replacement of native PsaD was determined not to be just a one-time event in that recombinant PsaD could be replaced further with newly synthesized recombinant PsaD. The PSI was still maintained its functionality even with the recombinant PsaD in place of the native PsaD. In other words, the ferredoxin had the same affinity for the PSI even when recombinant PsaD was in place of the native PsaD. The assembly was done *in vivo* in addition to all previous *in vitro* work and the PSI still functioned normally. These results suggest that PsaD is under constant maintenance as it is replaced periodically with other PsaD. A mechanism for the replacement has been

proposed where a new PsaD subunit will approach the PSI complex and electrostatically interact with the native PsaD at its surface. A transient dimer is probably formed from the two subunits, loosening the binding of PsaD with PSI, leaving the hydrophobic region of the newly synthesized PsaD exposed to an aqueous environment. This energetic incentive makes the external PsaD rotate and replace the native subunit. (Minai, *et al.* 2001).

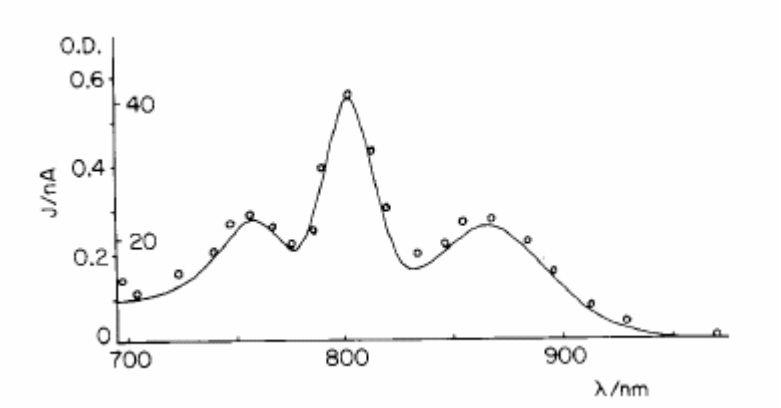

Figure 12: Comparison of the photocurrent action spectrum generated by an electrode modified with RC's via the thiol-binding reagent (dots) versus the reaction spectrum for native RC's (solid line). (Katz, 1993)

Similar work by Goldsmith, *et al.* with histidine tags has been performed on photosynthetic bacterial reaction centers. Making use of the high affinity of a genetically engineered poly-histidine (poly-His) tag and Ni-NTA (Nitrilo-Tri-Acetic acid) resin, one can bind proteins with this engineered tag to the Ni-NTA compound. Instead of tedious centrifugation steps, one can easily isolate bacterial RCs this way by simply adding a cell lysate to the resin, washing the resin to remove unwanted cellular contents and extracting the poly-His tag protein by displacement via an imidazole-containing buffer. In this case, the poly-His tag was introduced at the C-terminus of the M-subunit (Figure 14). Despite the alterations to the protein, the RCs are indistinguishable in most respects to the wild-type protein. The absorption spectrum of the modified RCs was very similar to that of wild-type RCs. The absorption spectrum is shown in Figure 13. Attachment of the poly-His tag on the M-subunit does not hinder the protein chemistry as the subunit is not involved in major tertiary or quaternary structural interactions with other residues. Addition of the poly-His tag also involved mutating a serine amino acid to an alanine amino acid. It was determined that this mutation did not change the protein chemistry either. In particular, it was determined that interactions with cytochrome *c* were not altered. However, the only change was a small difference in carotenoid composition. (Goldsmith, *et al.*, 1996)

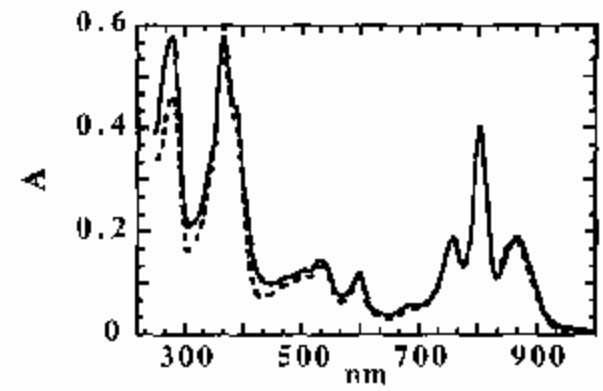

Figure 13: Absorption spectra of poly-His RCs after elution with buffer 3 on Ni-NTA (solid line) and after further purification on DEAE with an FPLC (dotted line). Note the spike near 800nm indicating strong absorption. (Goldsmith, *et al.*, 1996)

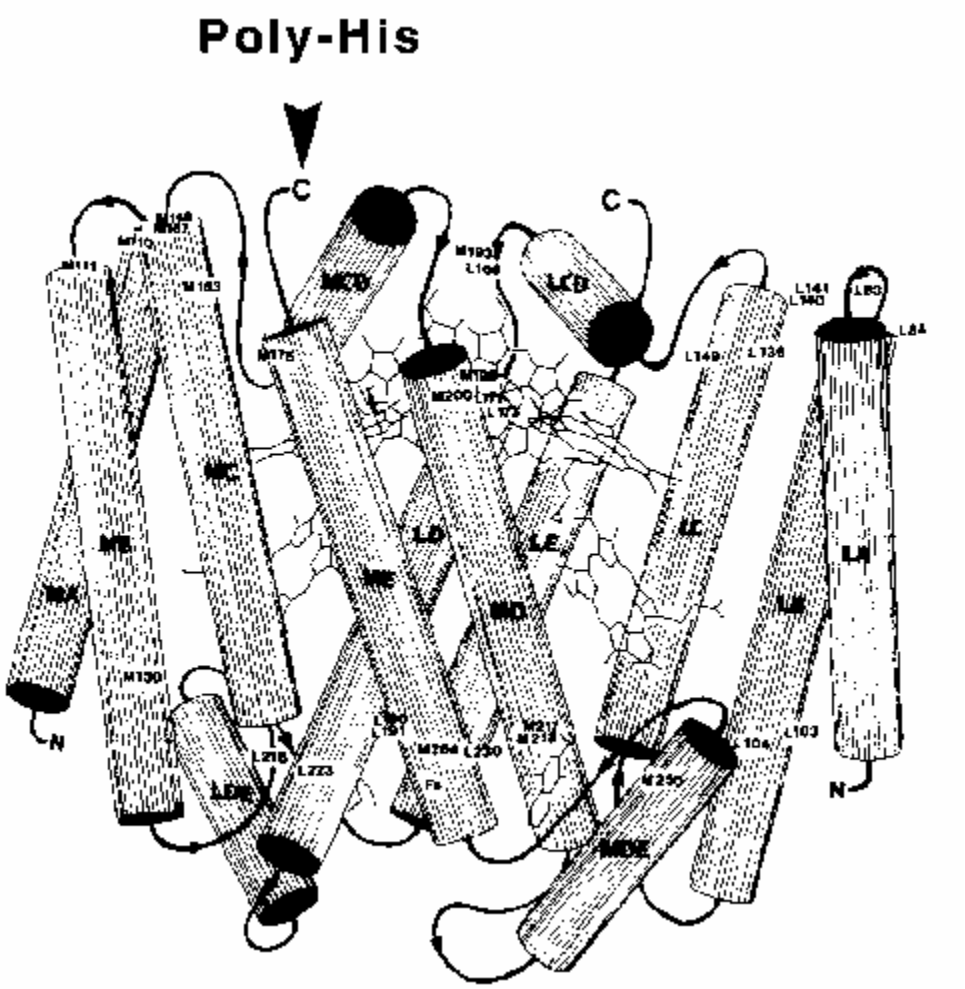

Figure 14: Schematic diagram of the L- and M-subunits of *Rp. viridis* RCs. The arrow points to the approximate position of the engineered poly-His tag at the C-terminus of the M subunit in the RC from *Rhodobacter sphaeroides.* (Goldsmith, *et al.*, 1996)

Work with biomolecular complexes can be viewed as a continuation of research into organic electronic devices. Organic electronic devices use more homogeneous layers of organic material and are better than standard semiconductor devices in certain applications. Devices made from biomolecular complexes may have similar properties to such organic devices. Multi-layered organic thin film devices, for example, have been demonstrated to act as photodetectors with high bandwidth, RC time constants of <200ps and a full width at half maximum of (720±70) ps. These devices have alternating layers of copper phthalocyanine (CuPc) and 3,4,9,10-perylenetetracarboxylic bis-

benzinimidazole (PTCBI) on an indium tin oxide (ITO) substrate. (Peumans, *et al.*, 2000) Other research has been conducted with CuPc/C_{60} photovoltaic cells. Such cells have power conversion efficiencies of (3.6±0.2)% under 1 sun global AM1.5 simulated solar illumination of 150mW/cm^2. This has been done by substituting PTCBI with the fullerene, C_{60}. It is anticipated such cells will lead to power conversion efficiencies in excess of 5%. (Peumans, *et al.*, 2001). Furthermore, research has been conducted on platinized chloroplasts, the cell organelle which houses many thylakoids. Colloidal platinum was precipitated onto photosynthetic membranes in aqueous solution, creating a material capable of sustained simultaneous photoevolution of hydrogen and oxygen when irradiated with visible light. In this experiment, it was concluded that the precipitated colloidal platinum directly contacted the reducing end of PSI such that the electron flow occurs across the biological membrane-metal interface with preservation of charge continuity and catalytic activity. (Greenbaum, 1985).

III. Self-assembly and Evaporation

The devices that are created consist of a transparent glass substrate with approximately 1600 Å of indium-tin-oxide (ITO), 10Å of titanium, 40Å of gold functionalized for the oriented assembly of binding PSI, 800Å of an organic semiconductor acting as a protective layer, and then 800Å of silver for contacts. The transparent ITO allows for a conducting substrate which also lets light excite the PSI or RCs. The protection layer is important because without it, the silver contacts would have to be directly deposited onto the fragile protein, destroying it. The protective layer is able to cover the protein without damaging it while also able to transfer charge between the protein and the contact. Preparing the devices takes several steps which can be divided into two categories: self-assembly and evaporation.

A. Self-assembly

Glass slides are obtained with ITO pre-deposited. However, due to the dust-creating cutting process, the slides are given a vigorous cleaning in sonicated distilled water and Micro-90 soap solution, sonicated acetone, boiling trichloroethane ($Cl_3C_2H_3$), more sonicated acetone, and boiling isopropyl alcohol (C_4H_9OH). This is followed by a five minute treatment under an ultraviolet lamp with ozone (O_3) present in order to eliminate any organic residue. Then, 10Å of titanium are deposited followed by 40Å of gold. The titanium serves as a sticking layer between the ITO and the gold. The layers are thin so that light can pass through to the photosynthetic complexes. After this, the slides are gently cleaned with acetone and isopropyl alcohol to remove any impurities

that may have fallen on the slides after removal from the electron-beam machine and then are again put under the ultraviolet lamp with ozone.

Next, the slides are treated with a series of chemicals in order to bind to the biomolecular complexes. First, a solution of 0.0408 mg Lomant's reagent is prepared in 10 mL isopropyl alcohol. The Lomant's reagent contains a disulfide which cleaves in the presence of a gold surface, forming two bifunctional molecules with both thiol and succinimidyl groups for coupling to gold and amines, respectively (see Figure 15). The gold slide is then put into this solution. After this, the slide is then rinsed in isopropyl alcohol and ethyl alcohol (C_2H_5OH) and then left to dry. Then 'NTA ligand' (see Figure 15) is prepared by dissolving 3.3 mg of NTA in 10 mL of distilled water. The NTA ligand is also bifunctional: its primary amine binds with the succinimidyl group of the Lomant's reagent and when charged with Ni^{2+}, its chelating ester groups bind with the 6 x Histidine tag that is found on the genetically engineered PSI. After the self-assembly of Lomant's reagent, the slide is left to soak in the NTA ligand solution, at T ~ 0°C in order to avoid denaturing the protein. Then, the slide is put in a nickel charging buffer (250mM nickel sulfate) for 30 minutes at room temperature. After this, the slide is put in a binding buffer (20 mM tris buffer at pH 7.8, 500 mM NaCl to reduce nonspecific binding of proteins, and 5 mM imidizole to cause the Ni from the charging solution to react) for 30 minutes as well. The slide then sits in a vial of genetically altered PSI and buffer for one hour. After the incubation is complete, the slide is rinsed in buffer and left to dry. The protein is not added to slides used as controls.

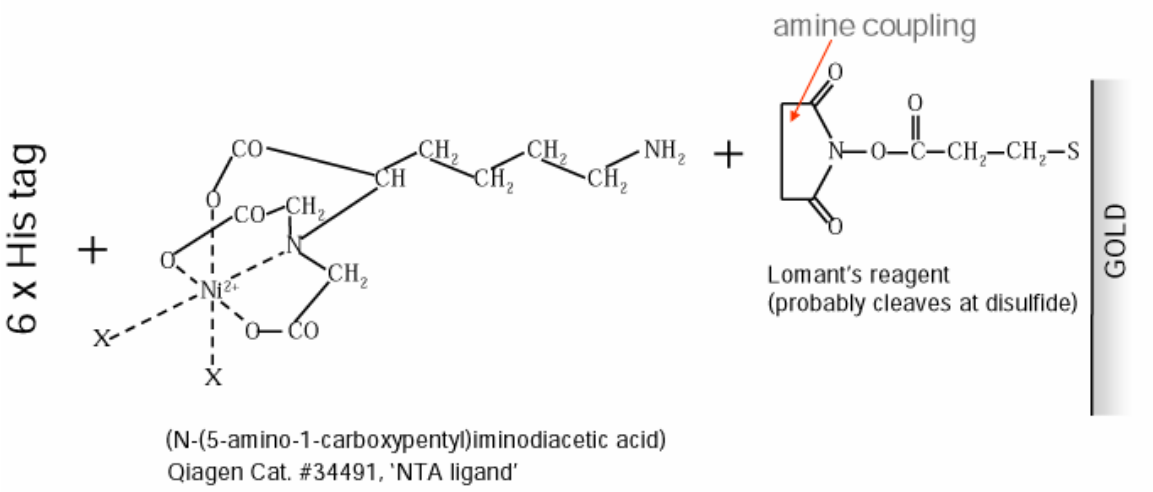

Figure 15: Diagram of binding of reagents used in self-assembly. The sulfur atom (thiol group) of the Lomant's reagent forms a bond with the gold substrate. Amine coupling between the Lomant's reagent and NTA ligand occurs. When the nickel charging buffer is introduced, the Ni^{2+} ion is bound to the ligand, which allows for the molecule to bind to the 6 x His tag of the genetically modified protein.

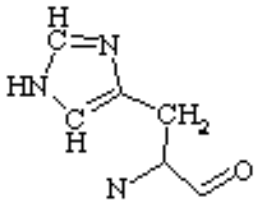

Figure 16: Structure of the amino acid, histidine (His). Six histidines are bound together at the end of PsaD, forming a tag which binds with NTA ligand. (<http://www.bio.davidson.edu/courses/Molbio/aatable.html>)

In some cases, spinning on a thin film was necessary. Spun-on films tend to retain more water than evaporated films. This can be useful for PSI since its native environment is aqueous. This spinner consists of a small stage with a rubber O-ring which surrounds a small opening. This opening is connected via a tube to a vacuum pump. When a slide is placed on the O-ring, a tight seal is formed via the vacuum pump, allowing the slide to be spun around at high angular velocities. A solution of the film material is placed via a syringe or dropper on the top of the slide until the solution covers all parts of the slide. The spin acceleration in RPM/second, spin velocity in RPM, and duration of spin are all specified and then the slide proceeds to spin according to the input

parameters. The end result is usually an extremely thin film of the material which is roughly evenly distributed over the slide.

Atomic force microscopy (AFM) images were taken to determine coverage of slides before evaporation. In some cases, a surface charge was characterized by applying a voltage to the AFM tip. Usually, AFM scans do not use any voltage when measuring the sample, which is PSI bound to gold in this case (Figure 17).

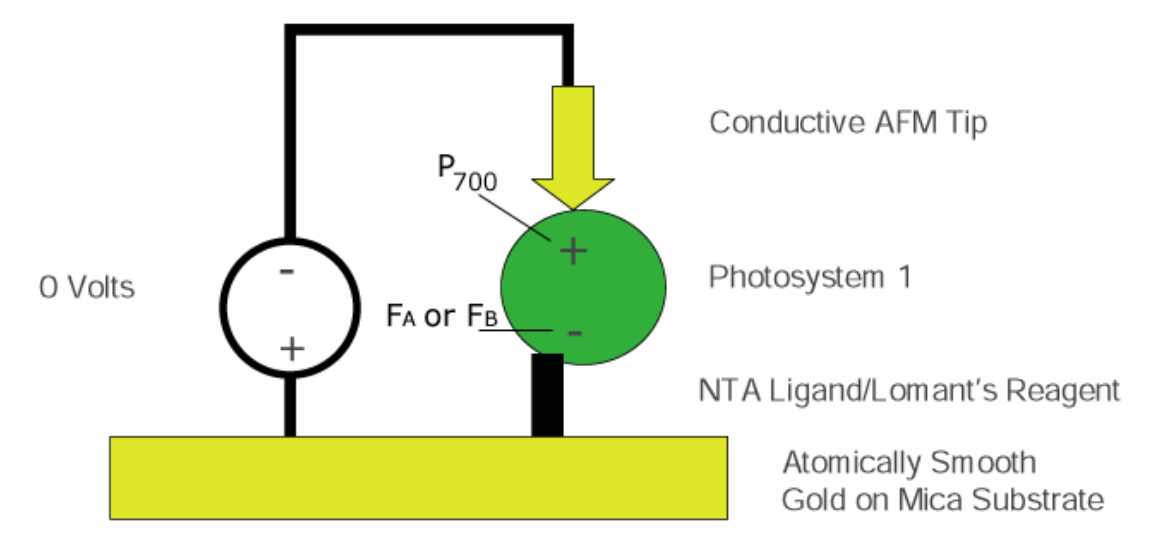

Figure 17: Schematic of setup for a normal AFM scan. The AFM tip (pictured as a gold arrow) probes the sample consisting of PSI attached to atomically smooth gold on mica via NTA Ligand and Lomant's reagent.

During normal operation, an atomic force microscope has a cantilever with a nanometer-size tip which measures the attractive or repulsive force between itself and the sample it is probing. The tip is continuously oscillating, "tapping" itself against the surface with a constant amplitude of oscillation. To maintain this amplitude, the cantilever's height is adjusted via a feedback loop. When the tip is brought close to a surface, Van der Waals forces and electrostatic forces affect the tip's height and hence, the measurement of the sample. So, as the driving frequency of the cantilever is swept through its resonant frequency, the phase shifts from being in phase (zero degrees) to out of phase (180

degrees) as shown in Figure 18. The phase difference can be measured with great precision. (Smith, 1994)

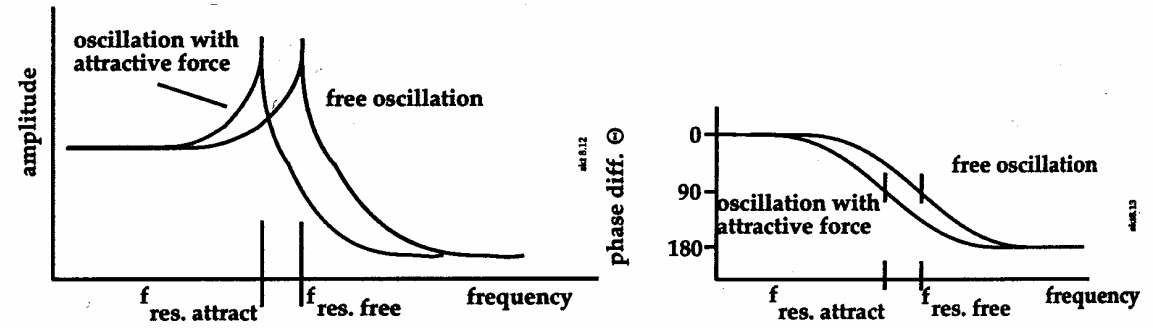

Figure 18: Diagram of phase and amplitude in relation to frequency of AFM cantilever oscillation. (Smith, 1994)

From this, the phase of oscillation and height of the "taps" are obtained. While performing a raster scan of the sample, a laser is focused on the cantilever and reflected into a highly sensitive photodetector. This is how the distance from the sample is measured. This laser generates light with a wavelength of 670nm, so some light is able to activate PSI occurring within close proximity to the AFM tip.

When the tip carries a charge, electromagnetic forces affect the distance between the cantilever and sample. The charge on PSI depends on the orientation: if the PSI is correctly oriented, then it has a positive charge on the end near the AFM tip. Thus, maximum attraction occurs when the tip has a negative voltage applied upon it and the PSI is oriented and excited.

PSI bound to a substrate via NTA Ligand and Lomant's reagent has the reducing end (stroma-facing end) of its electron transport channel oriented toward the substrate and the oxidizing end (lumen-facing end) oriented away from the substrate, towards the AFM tip. Thus, when a negative voltage is applied on the tip, a positive voltage will put onto the sample. Since the PSI is oriented such that it has a positive voltage measured

from its lumenal end to its stromal end, the effect of the biased AFM tip will add to this effect. In the end, the tip will have an affinity for positively biased objects and will tend to give higher resolution scans for regions with oriented PSI. This is due to the tip being drawn closer to the substrate and therefore oscillating closer to the substrate and sensing more detail in the structures. When the tip is given a positive bias, the opposite effect will occur. A negative voltage will be put onto the sample, counteracting the positive voltage found in the protein. The net effect is a repulsion of the tip near PSI, giving a scan of low resolution near the protein. The repulsion keeps the tip away from the surface, giving less detail on positively charged structures.

B. Evaporation

In order to grow some organic protective layers and a set of metal contacts on the PSI/RC layer, one must use an evaporator to create the nanometer-thick layers. For this project, a thermal evaporator was used. Thermal evaporators operate by heating up a container of source material called a "boat," such that the source material either boils or sublimes. This process is performed in a vacuum so the source material does not react with ambient gases. Vacuum conditions reduce the incorporation of impurities into the deposited film and the long mean free path at low pressures reduces collisions with ambient molecules, allowing the sublimed material to travel ballistically. Sublimed molecules must not aggregate, otherwise the film is not smooth.

Upon contact, the vaporized source material condenses into a solid film since the substrate surface is below the film's boiling or sublimation point. So, one just has to place the substrate in a position in the chamber that is not shadowed from the source boats. By including a thickness monitor in the chamber, the rate of deposition can be

ascertained. By rotating the substrate, the film is ensured to be uniform. The source boat in the evaporator is heated through resistive heating. A current runs through the boat, making the boat into a resistive circuit element which gives off thermal energy. Though it is theoretically possible to calculate the thermal power assuming all the energy in the boat is used in heating via $P = I^2R$, this is unreliable. So, the growth rate is obtained from a rate monitor. It is also known that increasing the current increases the boat temperature and growth rate.

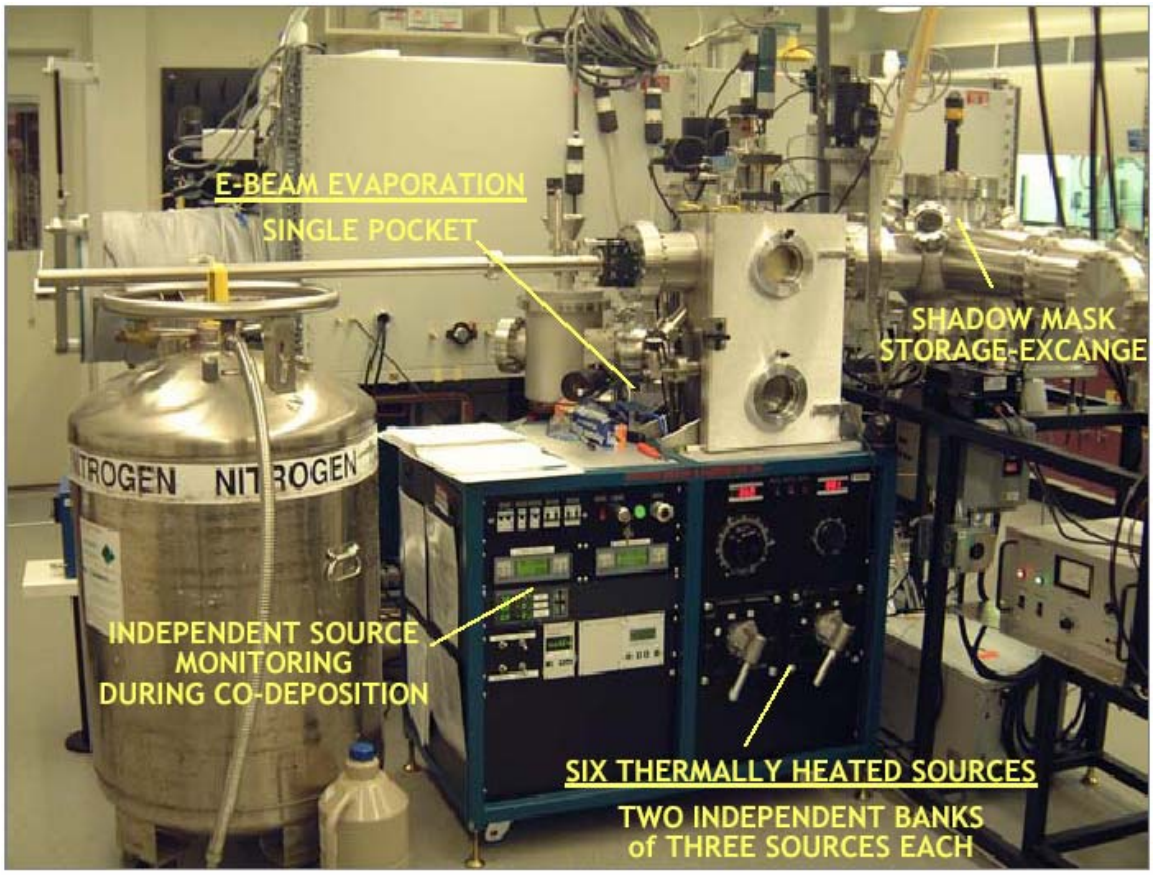

Figure 19: Picture of the thermal evaporator system used for growing thin films on substrates. It can hold up to six sources and can use a shadow-mask. (Bulović, 2003)

The system used in this evaporator (Figure 19) has two banks with three boats each. Each bank has a separate power supply. These boats are located at the bottom of the chamber whereas the substrate is face-down at the top of the chamber. There are

shutters which shield the substrate and another set of shutters that shield each bank. There are also two thickness monitors: one near the substrate and one near the left bank of the boats. The left bank of boats can handle a power load of up to 1.0 KVA and the right bank can handle a limit of 0.5 KVA.

The system is pumped down with a Leybold TW 300 Turbomolecular Pump acting as the turbo pump and a Boc Edwards ESDP12 Scroll Pump acting as the roughing pump. The roughing pump can pump the chamber down to between 1×10^{-1} to 1×10^{-2} Torr from atmospheric pressure. The turbo pump can then pump down the chamber to 1×10^{-6} Torr or lower which is required for evaporation.

IV. Photocurrent Measurements

In order to prove that PSI is part of the final system, it is imperative to take photocurrent measurements of the devices. The basic setup involves measuring the current from the device when it is excited by light and also when it is biased with a voltage. In order to perform these measurements, two setups are used: one which excites the device at a variety of wavelengths and another which obtains an *I-V* curve while the device is excited at one particular wavelength.

A. Spectrum Measurement

Measuring the spectrum of the device is important in order to establish that PSI is still intact and functioning in the final device. In order to do this, one must be able to excite the sample with varying wavelengths and measure the photocurrent of the device at each wavelength.

In order to do such a measurement, a variety of equipment is involved. The four main pieces of equipment are a monochromator, a current amplifier, and two lock-in amplifiers. The monochromator used is a Thermo-Oriel Cornerstone 670. It consists of a of a moveable grating that, lets only one wavelength of light through at a time. When a white-light source is shone on the input slit, any wavelength within the system's range can be output since white light consists of all wavelengths of light. The monochromator can output any wavelength of light from 190nm to 1100nm. The current amplifier multiplies the output current from the measurement of the sample by a gain and converts the current to a voltage. The lock-in amplifiers are able to isolate a weak signal and amplify it by use of a chopper. The chopper is able to turn a constant stream of light into

a series of pulses with a certain frequency. The lock-ins are able to use this frequency to perform a Fourier transform on the data and extract the weak signal, despite any background illumination.

In the final setup, the components are connected as shown in Figure 20. First, white light is generated from the Oriel lamp with a power of 220 Watts. This light is focused through a lens and projected into the Cornerstone monochromator. The output light of the monochromator is now of just one wavelength. This light is chopped, focused through another lens, and then focused through a beamsplitter. One ray out of the beamsplitter is focused onto the underside of the sample and the other ray is focused into a photodetector. One probe is touching the contact of the sample and another penetrates the organic protective layer and PSI layer, touching the gold substrate. With the contact probe as the signal and the substrate probe as ground, the signal is sent to the current amplifier. The current amplifier is able to put a bias on the sample if necessary, but it is mainly used to amplify the current by a fixed amount, converting the signal from current to voltage. This voltage is input into one lock-in amplifier. The lock-in also has the frequency of the chopper as one of its inputs and is able to extract the signal using this frequency. A series of measurements are taken for each wavelength of

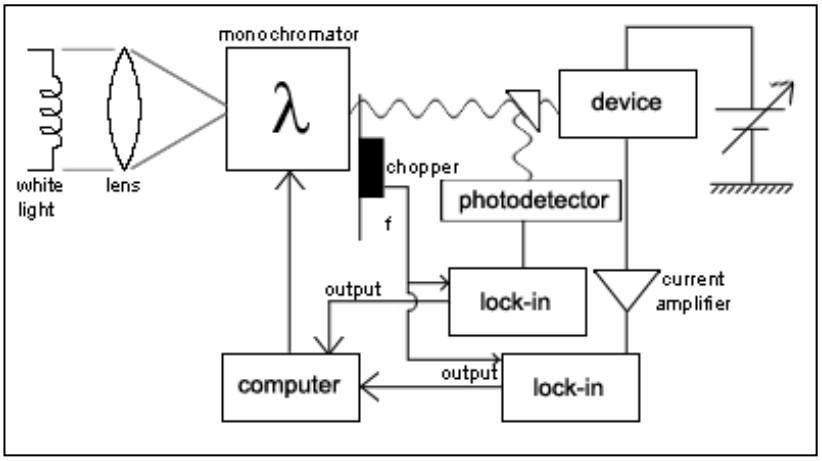

Figure 20: Component diagram of lock-in/monochromator setup.

light and are averaged via a LabVIEW program. The other lock-in takes in the signal from the photodetector via the current amplifier. The data from the contact is divided by this value in order to normalize the data for the nonlinearities in the white-light source and monochromator. The collected data must be corrected from the photodetector responsivity (Figure 21). The final data, after computing the number of photons per wavelength, gives the electrons out divided by the photons in per wavelength.

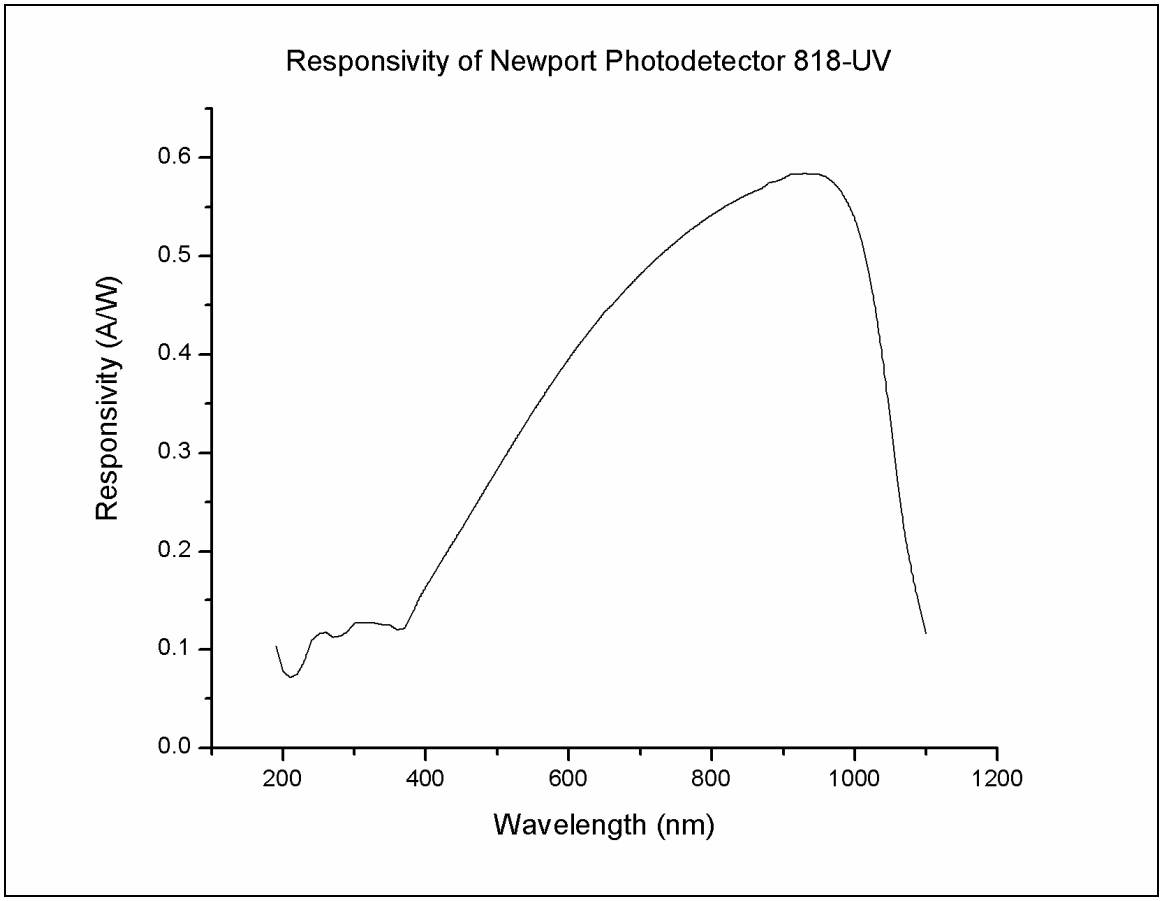

Figure 21: Responsivity of the 818-UV Newport Photodetector used in measurement. This data must be used to calibrate the data obtained in spectrum measurements. Note the quasi-constant data from 600nm to 800nm, where the PSI and bacterial RCs are most excited.

To reach the final calculation where electrons per photon versus wavelength is graphed, one must appropriately scale the obtained data. The raw data, *R*, is in units of Volts. When divided by the constant gain, *G*, in units of Volts/Amp, the raw data is converted to Amps, or electrons/second. The calibration data, *C*, obtained from the photodetector is in

units of Amps. When divided by the Newport Photodetector responsivity in units of Amps/Watt, one obtains the calibration data in units of Watts. This data in units of Watts can then be divided by the energy of the photon at each wavelength and can be converted to units of photons/second. Dividing the converted raw data by the converted calibrated data gives a final number in units of electron/photon (Equation 1). Though the responsivity and wavelength itself are wavelength dependent, when divided by each other for this calculation, the value remains roughly constant over the range from 600nm to 800nm as shown in Figure 22. This means that the shape of photocurrent measurements will stay about the same after full calibration for measurements over the range from 600nm to 800nm.

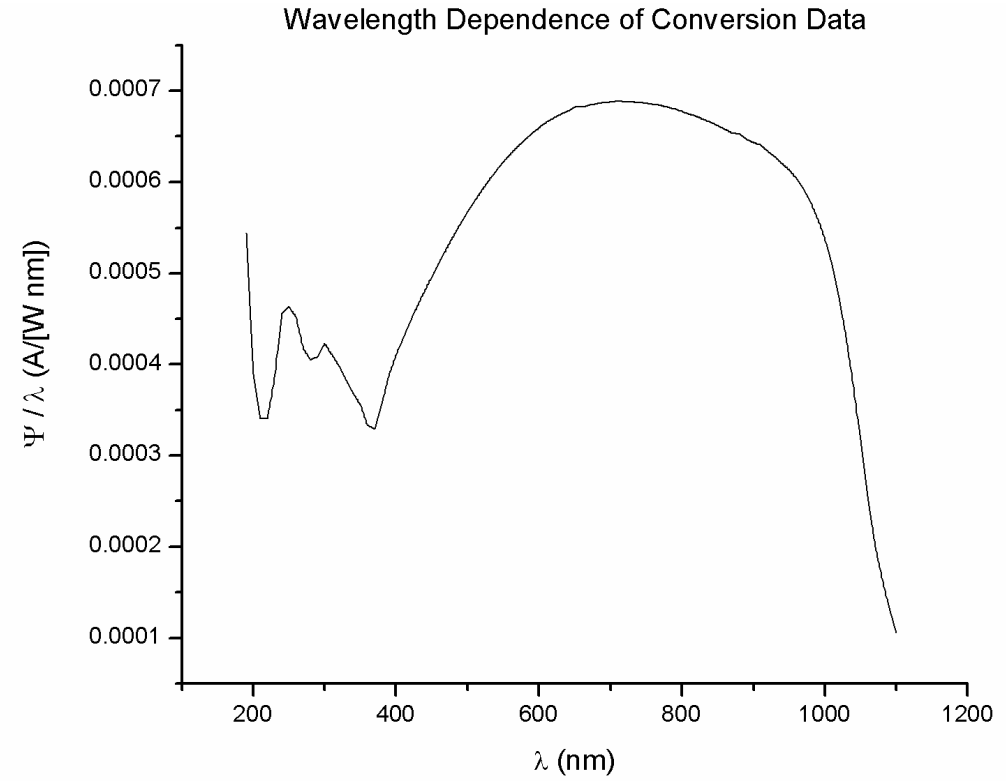

Figure 22: Photodetector responsivity, Ψ, divided by wavelength, λ, versus wavelength. Note the roughly constant value from 600nm to 800nm.

$$\frac{\frac{R}{G}}{\frac{C}{\Psi\left(\frac{hc}{\lambda}\right)}} = \left(\frac{R}{C}\right)\left(\frac{\Psi}{G}\right)\left(\frac{hc}{\lambda}\right) = f(\lambda)\left[\frac{electrons}{photon}\right]$$

Equation 1: Calculation of the calibration of a device such that the final wavelength-dependent data, $f(\lambda)$, is in units of electrons/photon. Note that the only wavelength dependent terms are Ψ and λ and when divided by each other, are roughly constant of the desired range of calculation. R is the raw data, G is the gain, C is the calibration data, Ψ is the photodetector responsivity, h is Planck's constant, c is the speed of light, and λ is the wavelength.

The LabVIEW program is able to change the wavelength of the monochromator and perform computations on the lock-in measurements and save all the data to a file. The program first applies the user's settings to the lock-ins. The user can set the sensitivity and time constants as well as other variables. Then the user decides the initial and final wavelengths as well as the increment. The user also selects how many samples to take and average for each wavelength. Each average is stored in an array of values along with the standard deviation and wavelength. The program then divides by the data received from the photodetector. This normalizes the data by the white light source and the beamsplitter. After the program reaches the final wavelength, the user is able to save the raw data and the photodetector-normalized data. The program also has a feature where the user can open any tab-delimited text spreadsheet and graph the contents (See Appendix for more details).

Synchronous detection improves the sensitivity of photocurrent measurements. In order to do this, the lock-in amplifier uses phase-sensitive detection (PSD) in order to single out the component of the total input signal at a specific frequency and phase. All other components at different frequencies are rejected. In order to perform phase-sensitive detection, the measurement requires a reference. In this setup, the chopper's spinning frequency is the reference. The response of the signal is also at the chopped

frequency. So, if the reference has a frequency of ω_r, then the signal also has the same frequency. If we let the signal be a sine wave for explanation purposes, then its function would be $V_{sig}\sin(\omega_r t + \theta_{sig})$. The lock-in would generate its own sine wave with the function $V_L\sin(\omega_L t + \theta_{ref})$. The output of the PSD is the product of these waves:

$$\begin{aligned} V_{psd} &= V_{sig}V_L\sin(\omega_r t + \theta_{sig})\sin(\omega_L t + \theta_{ref}) \\ &= \tfrac{1}{2} V_{sig}V_L\cos([\omega_r - \omega_L]t + \theta_{sig} - \theta_{ref}) - \\ &\quad \tfrac{1}{2} V_{sig}V_L\cos([\omega_r + \omega_L]t + \theta_{sig} + \theta_{ref}) \end{aligned}$$

Equation 2: Calculation of V_{psd}.

Now the PSD's output is two AC signals, one with a frequency $(\omega_r - \omega_L)$ and one with a frequency $(\omega_r + \omega_L)$. Then, the signals are passed through a low pass filter, removing all rapidly changing signals, e.g. all AC signals. This means an output of zero, unless ω_r equals ω_L. Then there is no time-component to V_{psd} and it becomes a DC signal which will not be removed by the low pass filter. So now V_{psd} is $\frac{1}{2} V_{sig}V_L\cos(\theta_{sig} - \theta_{ref})$. This DC signal is proportional to the signal's amplitude. Now, if the signal has noise, the noisy parts of the signal will be attenuated by the low pass filter if they are at frequencies far from the reference frequency. The attenuation depends on the low pass filter's bandwidth and roll-off. The lock-in reference must be phase-locked to the signal reference, otherwise $\cos(\theta_{sig} - \theta_{ref})$ will change and V_{psd} will not be a DC signal. Phase-locking the two signals is done through a phase-locked-loop (PLL) which actively tracks the external reference signal. Additionally, a lock-in with just a cosine dependence will not give the full signal by itself. For example, if $\theta_{sig} - \theta_{ref}$ is 90°, then V_{psd} will be zero and no signal can be ascertained. So, A term proportional to $V_{sig}\sin(\theta_{sig} - \theta_{ref})$ is used. The lock-in then has 2 outputs, one that can show $X = V_{sig}\cos\theta$ and one that can show $Y = V_{sig}\sin\theta$, where $\theta = \theta_{sig} - \theta_{ref}$. The mode can also be changed such that $R = V_{sig}$ and θ

are shown. This way the signal and the phase lag can both be measured. (Stanford Research Systems, Inc., 2002).

B. Laser Measurement

Another apparatus to measure photocurrent involves a laser that emits concentrated light at one wavelength onto the measured sample. The increased intensity of light upon the sample gives more pronounced differences between measurements taken with the laser light off and measurements taken with the laser light on. Furthermore, if the wavelength of the laser matches the peak absorption wavelength of the protein used in the device, very pronounced differences can occur.

The setup for this measurement is simpler than the measurement across the whole spectrum of wavelengths. A laser is setup on an adjustable mount where it can be finely adjusted to focus on a particular device on a slide containing an array of devices. The contact and substrate of the device are attached to an HP4156 analyzer. On the analyzer, the device's I-V characteristic can be easily ascertained. For the measurement of devices, the voltage range was from -2V to +2V with an increment of 50mV. The compliance is set to 1mA so if the signal is greater than this, the measurement will stop. This safeguards the device from shorting out during initial measurements.

C. Results

Experiments conducted involved creation of devices on slides and then measurements of slides using the schemes described in the experimental setup. In the end, the basic device structure consists of glass, ~1600Å ITO, 10Å titanium, 40Å gold, surface functionalization chemicals, oriented PSI or bacterial RCs, an organic charge

transport layer, and then an 800Å silver contact (Figure 23).

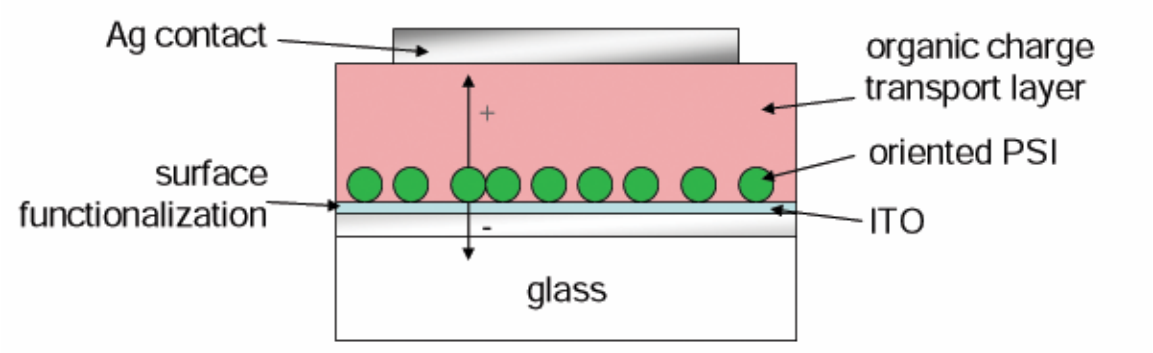

Figure 23: Cross-section of one of many devices appearing on a ½" by ½" slide. (not to scale)

In order to determine satisfactorily whether PSI covers the substrate upon reaction, atomic force microscopy (AFM) scans of the surface are taken. Results from this show the presence of oriented PSI. After the devices are created via an evaporated protective layer or spun-on film, then measurements are taken to determine if the device generates photocurrent from the PSI.

i. Atomic Force Microscopy and Surface Characterization

Results from AFM images show dense coverage of substrates. However, it is impossible to deduce definitively from normal AFM images whether the coverage results directly from PSI. Figure 24 shows phase images for amine-coupled PSI and protein exchange-coupled PSI. The amine-coupled PSI is bound to Lomant's reagent which is in turn bound to a gold substrate. Since there are many places for amine coupling to occur, the PSI proteins are most likely not uniformly or quasi-uniformly oriented. The exchange-coupled PSI is bound to NTA ligand via a PsaD group genetically engineered to have a 6 x His tag. The NTA ligand is bound to Lomant's reagent which is bound to gold. This is called "exchange-coupled PSI" since the PSI exchanges PsaD subunits with the genetically modified PsaD anchored to the gold substrate via NTA ligand and

Lomant's reagent. (Minai, *et al.*, 2001) After the exchange, the PSI's stromal-facing end is directed toward the gold substrate, creating what is presumed to be a uniformly oriented layer of PSI. Though the phase images of the AFM scans only show the density of coverage, it can be seen that there is a different density of coverage for the two treatments. This would indicate that protein exchange-coupled PSI tends to more sparsely populate the substrate than the amine-coupled PSI.

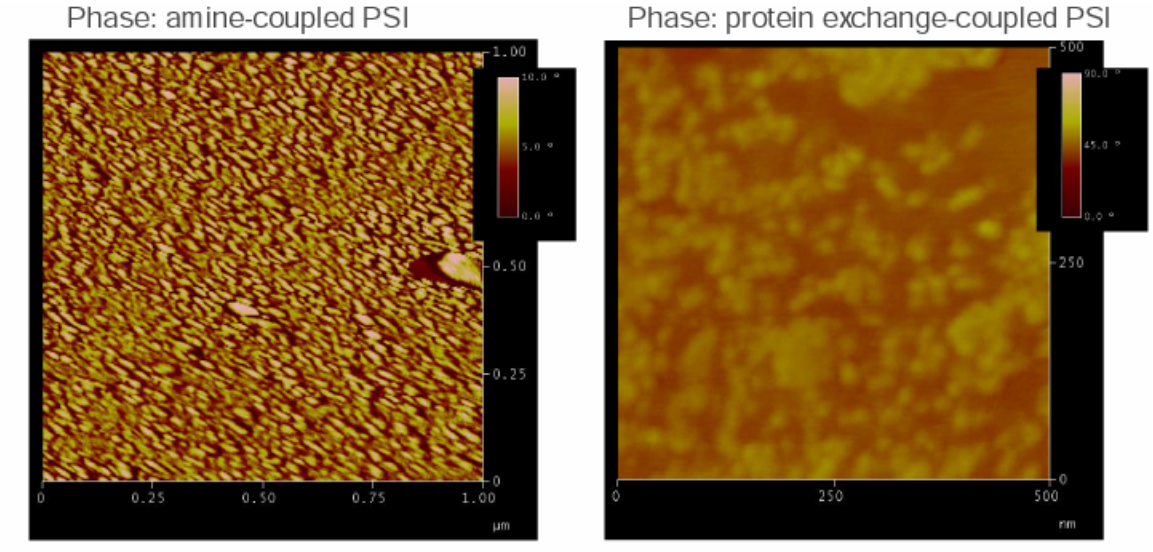

Figure 24: Atomic force microscopy phase images of net coverage of PSI on atomically flat Au on mica. The amine-coupled PSI (left) probably has no net orientation whereas the protein exchange-coupled PSI (right) probably has a net orientation. Amine coupling via Lomant's reagent shows nearly 100% surface coverage. Protein-exchange coupling shows less coverage (note change in scale)

AFM's shortcoming in definitively showing the presence of PSI can be remedied by making the tip voltage-sensitive and using a 670nm wavelength laser to excite the PSI. It has been shown that negative tip voltages increase the resolution of scans around areas which themselves have a negative voltage when compared to ground. Figure 25 shows the change in phase during one such voltage sensitive scan. In one area of the -1V scan, three particles in a triangular pattern can be seen. This would indicate the presence of PSI since each particle has a diameter of 10nm and a negative voltage when excited, and

also because the particles occur in what appears to be a trimer which PSI has been known to form.

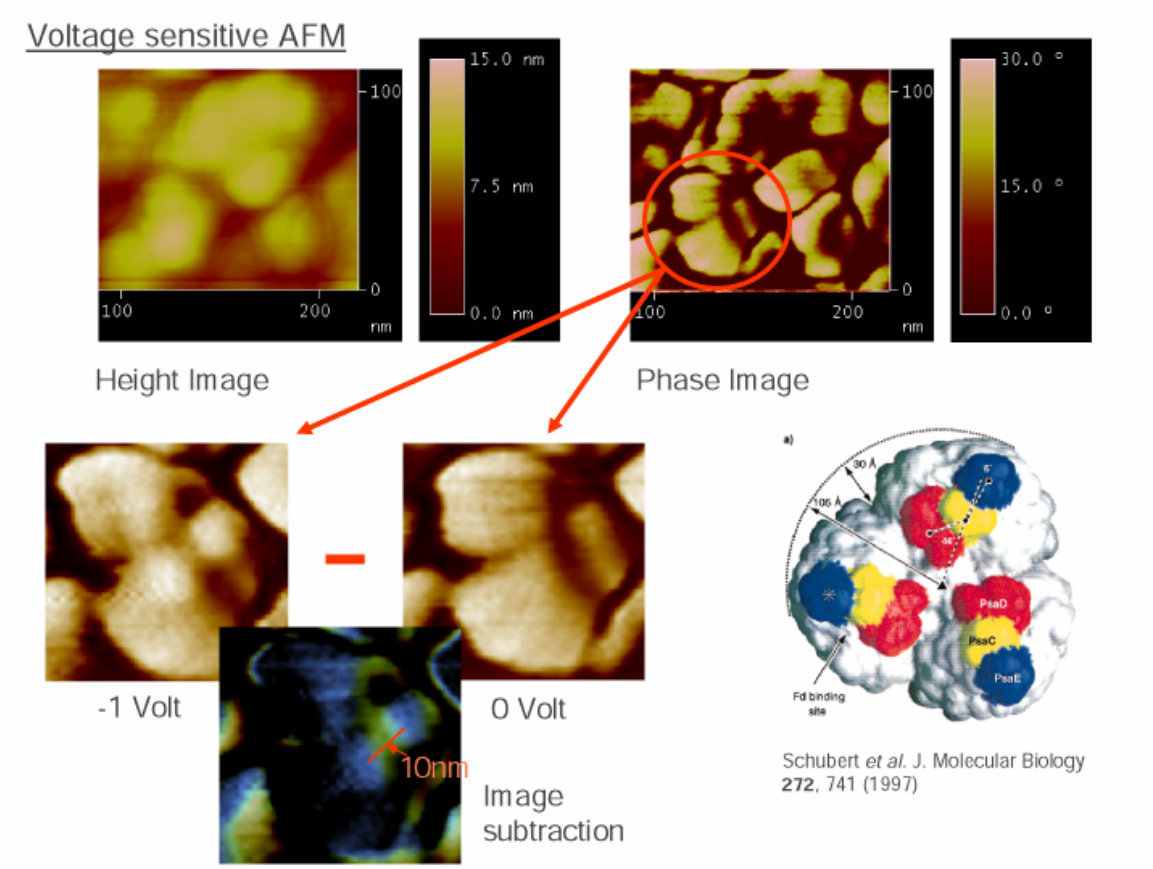

Figure 25: Voltage sensitive AFM of PSI bound to a gold substrate. Note the pronounced trimer in the -1V scan that is barely visible in the 0V scan. Image subtraction reveals a 10nm area with a large amount of activity (seemingly active regions on the edges are due to edge-translation effects). (Data courtesy of Julie Norville)

Other regions of the AFM scan show the presence of trimers. Differences between the -1V scan and the 0V scan are shown in boxes in Figure 26. Many regions show changes in activity with the change in voltage. Many active regions are trimers located in regions with heights of about 10nm (Figure 27). Many sets of trimers lie within the same plane indicating a strong likelihood for oriented PSI since the trimers consist of PSI bound in such a way that they all face in the same direction and the plane of binding is roughly parallel to the substrate surface. They are likely to be oriented

stromal side-down rather than stromal side-up since the binding reagents bind to PsaD, a stromal subunit.

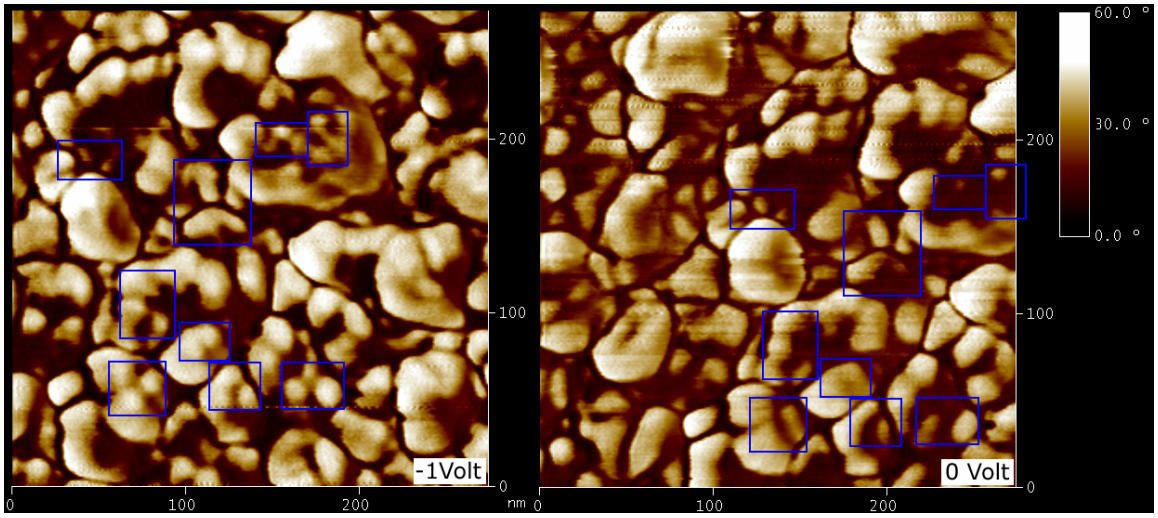

Figure 26: Location of PSI trimers on a -1 Volt phase scan and a 0 Volt phase scan. Boxes in one image correspond to boxes in the other. Note the prominence of trimers in the -1 Volt scan and the reduced appearance in the 0 Volt scan. Each particle in the trimer has a diameter of roughly 10nm. (Data courtesy of Julie Norville)

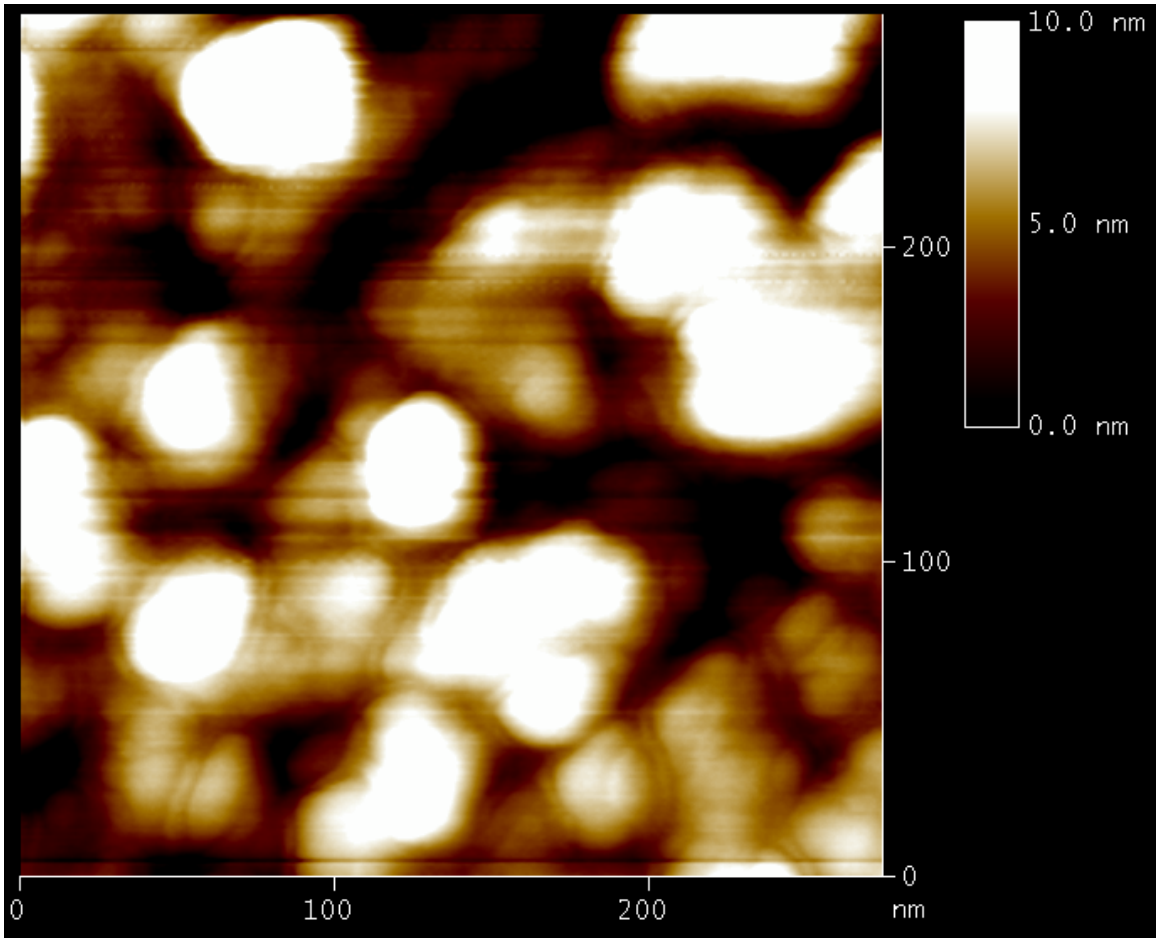

Figure 27: Height image of sample. Note the decrease in detail and the correspondence to the phase image. Many candidate trimers are located near clusters with heights of about 10nm, the diameter of PSI. (Data courtesy of Julie Norville)

Images taken with a positive tip voltage do not show much difference from the unbiased scans. The reason for this voltage dependence is unclear, but it could be due to a substrate surface charge or the repulsive effect between the tip and the protein. The surface has negative and positive charges localized to small areas, but this implies there is no net charge. These small charges could be from the residual charges of the hydrophilic surface of PSI. Another possibility is a photoinduced charge that creates a positive charge if oriented correctly, implying the existence of a net charge. Figure 28 juxtaposes the two images as well as their subtraction. The subtraction does not show any remarkable differences between the two scans, unlike the difference between the 0V and -

1V scans shown in greater detail in Figure 29. The apparent trimer can be seen in the subtraction image as three 10nm diameter lobes in a triangular pattern.

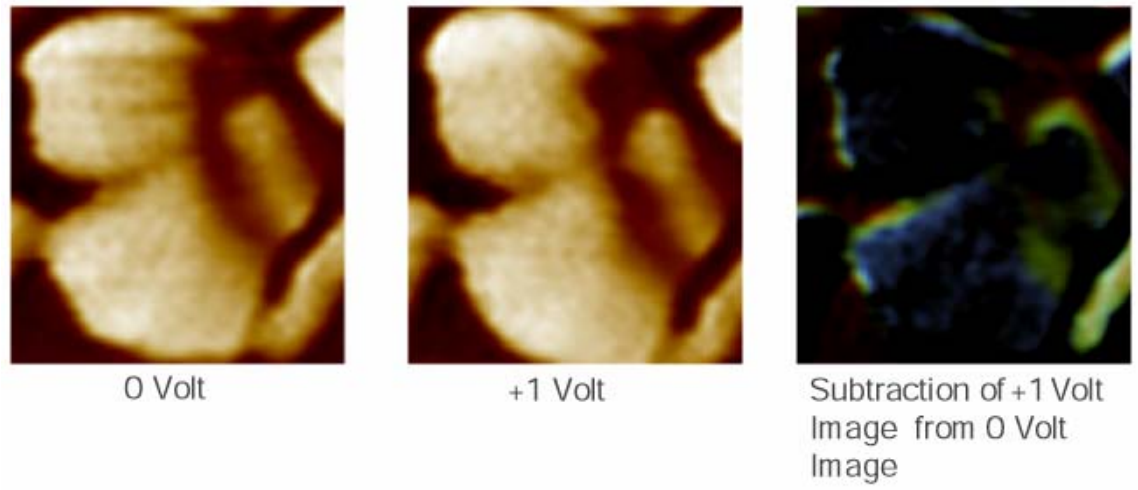

Figure 28: Comparison of scans taken at 0 Volts and +1 Volt.

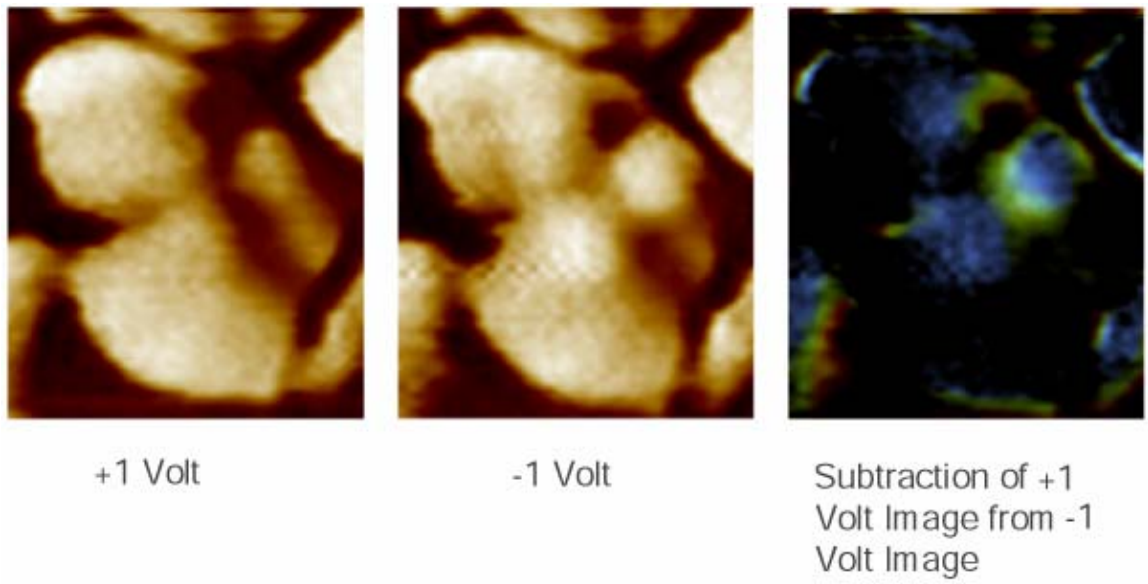

Figure 29: Comparison of scan s taken at +1 Volt and -1 Volt. Note the pronounced 10nm long region of activity.

Other active areas are shown in Figure 30, Figure 31, and Figure 32. Again, the subtraction images highlight the changes between scans. Locations of the areas in question are circled on the 0V image in Figure 30 and Figure 31 and on the -1V image in Figure 32.

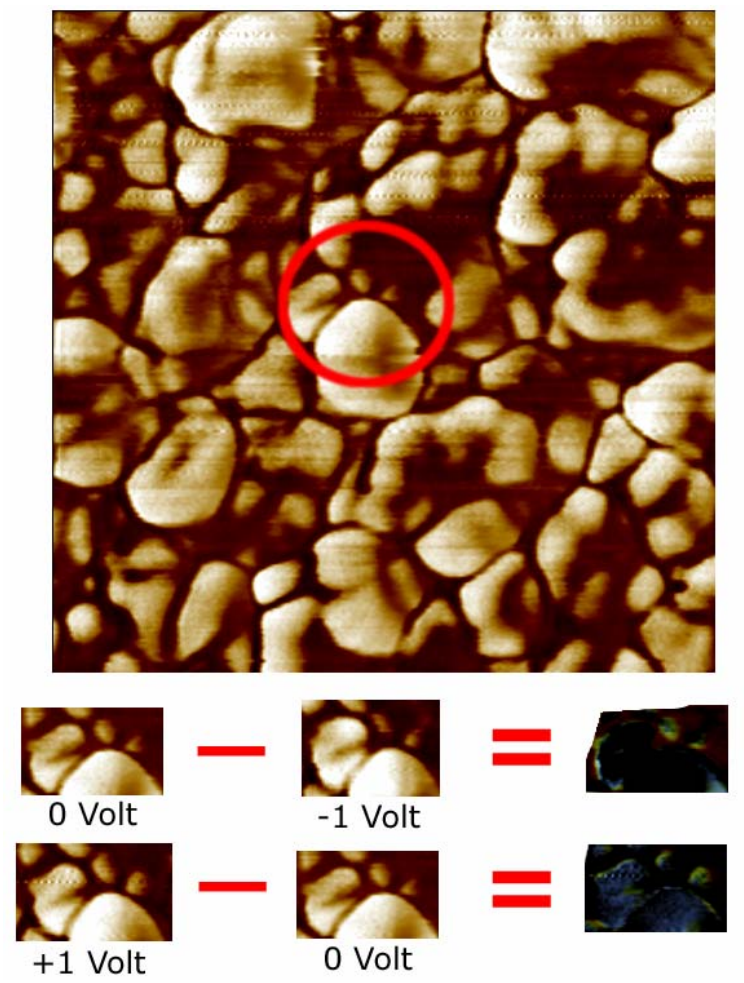

Figure 30: Subtraction of images for circled area of a 0 Volt phase scan. The two spherical particles show great change indicating they are most likely PSI protein.

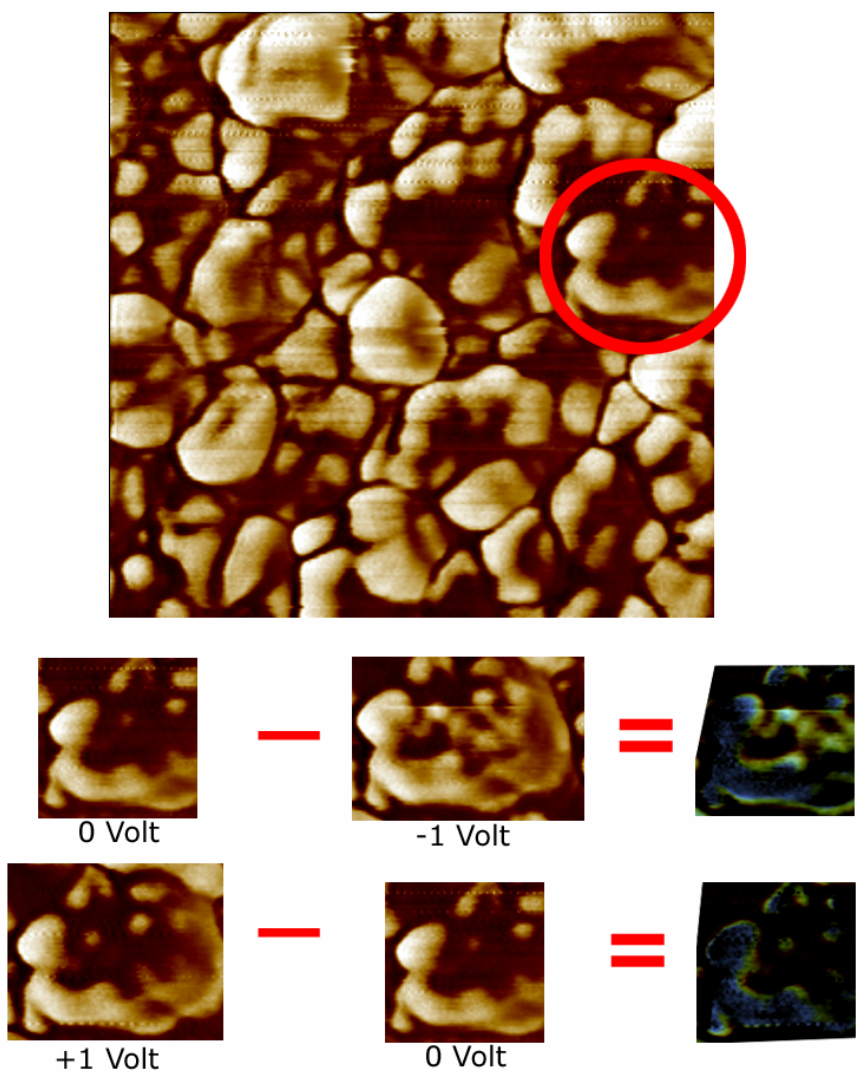

Figure 31: Subtraction of images for circled area. Note the large difference between the 0 Volt scan and the -1 Volt scan. This is a candidate trimer. The trimer is circled on a 0 Volt phase scan.

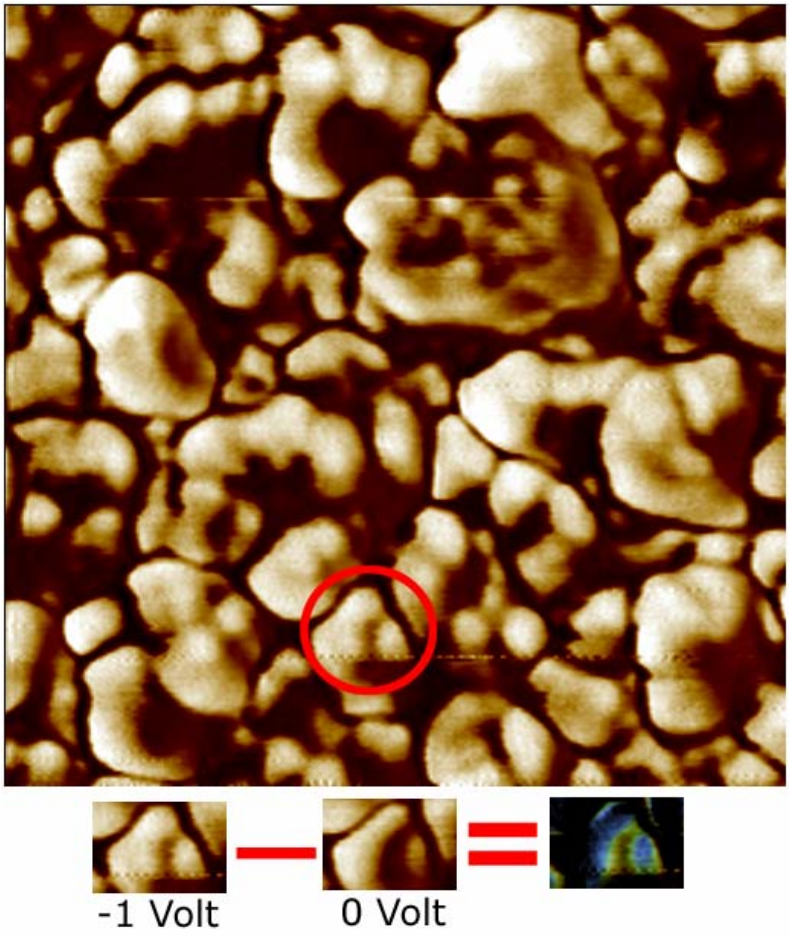

Figure 32: Subtraction image for another trimer. Note the strong difference in scans for this trimer. The source trimer is circled on the -1 Volt phase scan image.

This voltage-dependence of scans is either a result of conduction or a photo-effect from PSI complexes. To determine definitively whether conduction is playing a role, voltage sensitive AFM measurements should be taken where the PSI is unoriented or where the substrate is an insulator. If there is indeed a photo-effect, it is likely due to the PSI complexes and their orientation. When photo-excited, the oriented PSI have their positive lumenal end close to the AFM. A negative tip probably attracts this charge (P_{700}^{+}) away from the fixed negative charge on the stromal end of the protein, giving an image with a large phase difference. A positive tip probably pushes the charge toward the fixed negative charge, decreasing its effect. This would give a phase difference of a

lesser magnitude. This asymmetric behavior between positive bias and negative bias makes the PSI behave like a diode circuit element (Figure 33).

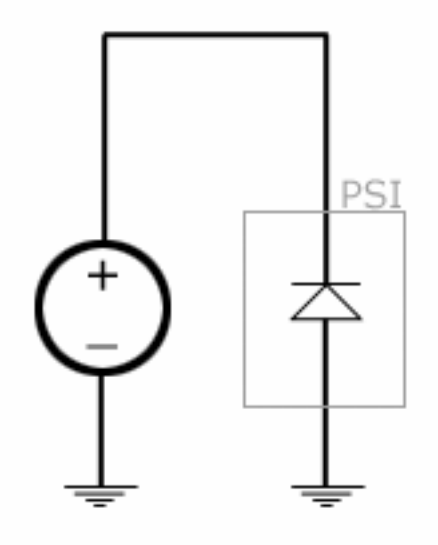

Figure 33: Diagram representing the voltage sensitive AFM (the voltage source) and the PSI (the diode). Note when the AFM tip is positive, current does not flow, but when it is negative, a response can be seen.

In addition to voltage sensitive AFM scans, the presence of PSI can be determined via measurement of an absorption spectrum. Different chemicals and proteins maximally absorb different wavelengths of light. Due to the high chlorophyll content of PSI, it has an absorption peak near 700nm as shown in Figure 34. PSI also has another absorption peak near 425nm. When PSI is added to a buffer containing triton, a detergent, the absorption spectrum shows peaks at 425nm and 700nm as shown in Figure 35. This indicates at least the presence of chlorophyll, but does not indicate anything about the intactness of the protein. Three out of four scans of the PSI bound to a gold substrate, or solid state PSI, show strong peaks near 425nm and 700nm. The material in the fourth scan may have unsuccessfully bound to the substrate or may have become denatured. In the solid state devices, the 425nm peak is less pronounced, indicating that the process by which the PSI is bound to the substrate might affect the absorption of PSI.

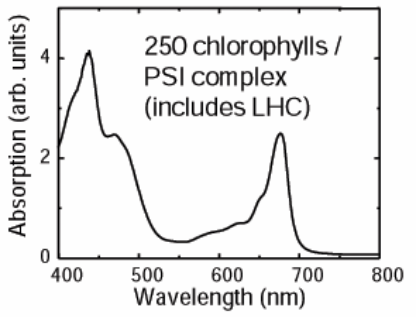

Figure 34: Absorption spectrum of PSI complex along with some light harvesting complex (LHC). Note the peaks near 425nm and 670nm.

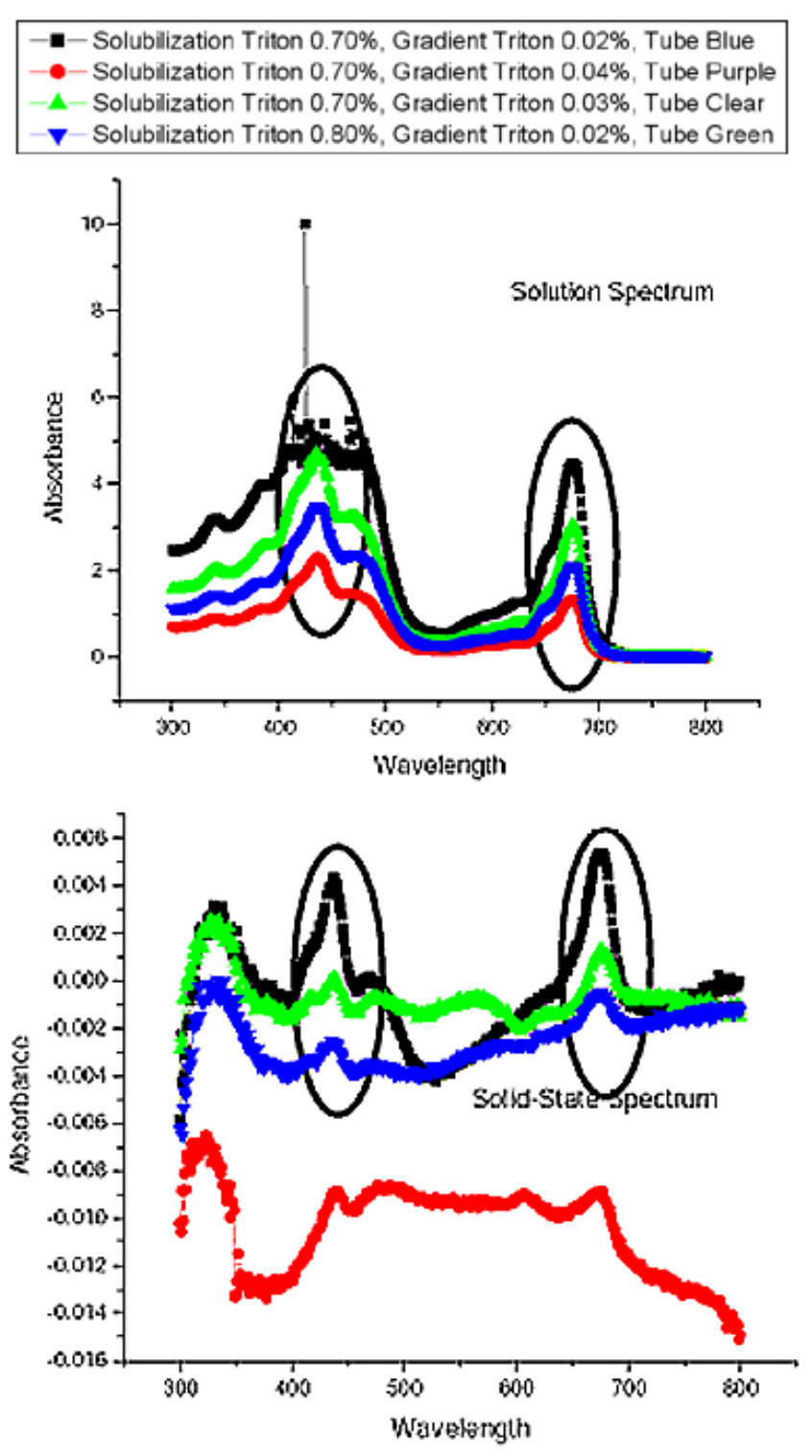

Figure 35: Evidence that PSI is maintained through spectral response. Different curves show solubilization of triton and gradient of triton, a detergent. Absorption peaks are near 425nm and 670 nm. Left graph shows solution spectrum and right graph shows solid state spectrum. (courtesy of Julie Norville)

ii. Thermally Evaporated Protective Layer Device Data

After chemically binding PSI to a substrate, a protective layer must be applied to the device. This layer can be affixed by many means, including thermal evaporation. The layer itself must not damage or chemically alter the PSI and it must also be able to conduct, as the lumenal side of the PSI is directed toward the protective layer. In most experiments, Alq_3 (Figure 36), an electron-transporting organic molecule, is used as the protective layer. Copper phthalocyanine (CuPc) (Figure 37) is a hole-transporting organic molecule used for thermal evaporations. Alq_3 has maximum absorption peaks at wavelengths which are not near 700nm, the key absorption peak for PSI and chlorophyll. CuPc, on the other hand, has an absorption peak around 680nm which is very close to 700nm.

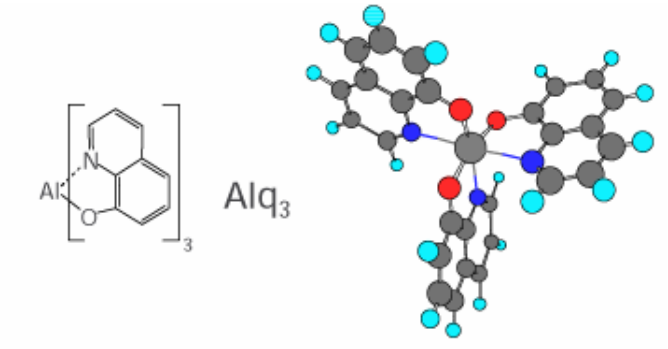

Figure 36: Structural formula and ball-and-stick model of the electron-transporting organic protective layer material Alq_3. In the ball-and-stick model, gray corresponds to carbon, save for the central aluminum atom, cyan corresponds to hydrogen, red corresponds to oxygen, and blue corresponds to nitrogen.

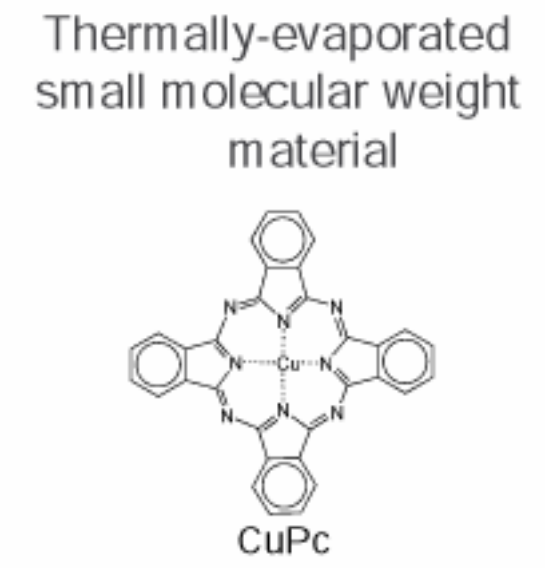

Figure 37: Structural formula for copper phthalocyanine (CuPc), an electron-transporting organic protective layer material.

An initial *I-V* characterization result of an unoriented PSI device is shown in Figure 38. This device had an 800Å Alq_3 protective layer on top of PSI obtained from Barry Bruce bound only to Lomant's reagent which was bound to a gold substrate. Measurements taken in the dark and in the presence of a 5mW 670nm laser show a relatively large difference for negative voltages.

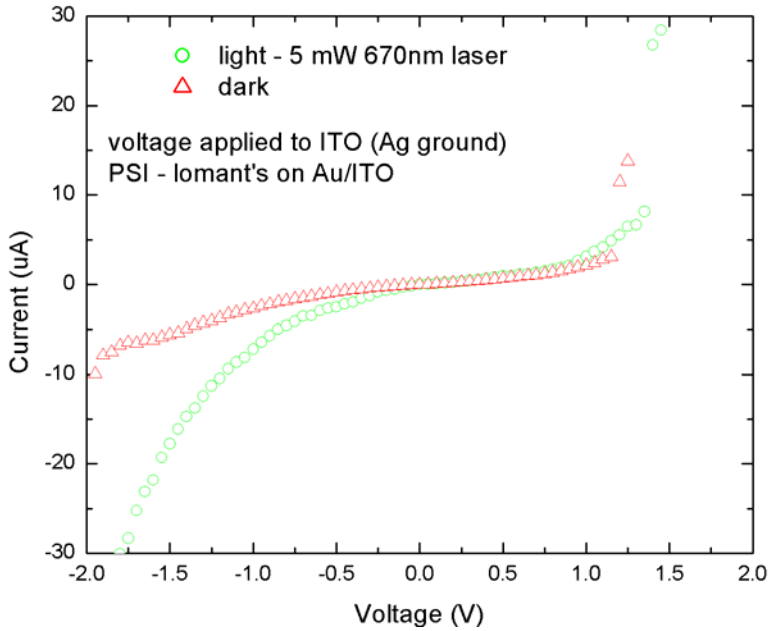

Figure 38: Current-voltage response of a PSI device with an Alq_3 organic protective layer. Note the

stronger response in the presence of 670nm laser light.

For this measurement, one probe, the ground probe, was in contact with the substrate and the other was in contact with the device cathode. While excited, the device draws more negative current for a negative bias than when it is unexcited. This implies there is a flow of electrons from the cathode toward the substrate which is amplified in the presence of light. A possible explanation is that the light excites the P_{700} in the PSI, causing it to donate an electron, passing it eventually to F_A or F_B, the Fe_4S_4 clusters in PsaC, a stromal subunit. The P_{700} becomes positively charged as a result and is reduced by the current flow through the silver contact and Alq_3 protective layer. As the light continues to shine, the oriented PSI induce more current to flow. An alternate explanation is that the photocurrent may arise from photo-enhanced injection at an interface. In this process, absorption of a photon excites an electron, enabling it to "jump" an injection barrier, thereby increasing the current. To determine which effect is responsible, an action spectrum must be taken.

Another device's *I-V* characteristic was measured as shown in Figure 39. This device had slides covered in 150 μL of 6mg DTSSP (3,3´-Dithiobis(sulfosuccinimidylpropionate), a form of Lomant's reagent)/mL H_2O and then PSI obtained from Barry Bruce. This device also contained unoriented PSI. While measuring this device, a result similar to that shown in Figure 38 was found where excited devices had greater negative current flow while negatively biased. The device was first measured in the dark four times (see the plots labeled DarkI-1 to DarkI-4). Then it was measured in the presence of 670nm laser light five times (see the plots labeled LightI-1 to LightI-5). Then a couple more measurements were taken in the dark and then more in the light (see the plots labeled DII/LII-1 to DII/LII-7). Since the excited

and unexcited data in the DII/LII series was indistinguishable, it was all lumped into one group. The LightI group can be seen more clearly in Figure 40. This data shows that the devices decay after an initial illumination with the laser. This decay could be due to the laser being too intense and breaking up the structures or some charge retention by the PSI after excitation. Since there is no ferredoxin carrier to transfer away negative charge at the stromal interface, the charge might be retained on PSI, enhancing protein degradation. For a positive bias, this device shows a positive current flow. The plot LightI-3 decays to a plot similar to one taken in the dark at a bias of about +1.5V. This device has been calculated to have a 10% external quantum efficiency.

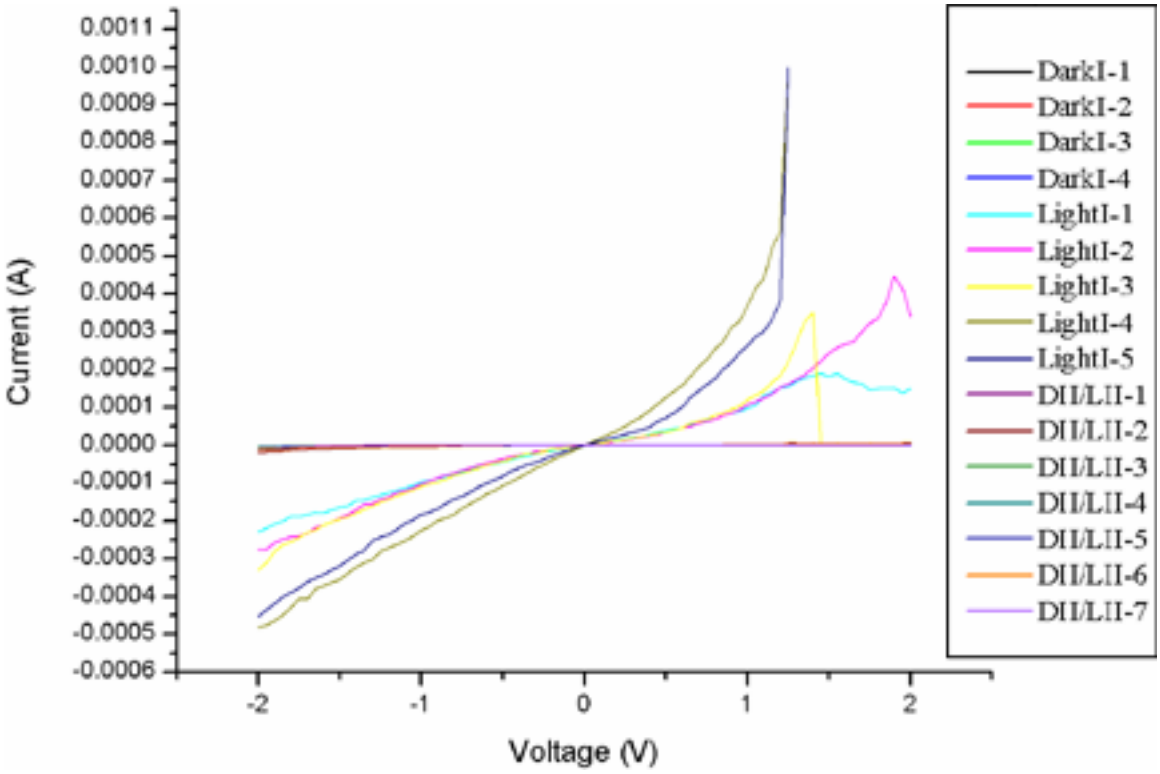

Figure 39: Response from an unoriented PSI device with an organic protective layer of Alq_3. The band of values with a value differing by almost two orders of magnitude was taken when 670nm laser light was focused on the sample. Subsequent data taken in the dark and with the laser light was within the range of values taken in the dark before the laser was turned on. This shows a 10% external quantum efficiency.

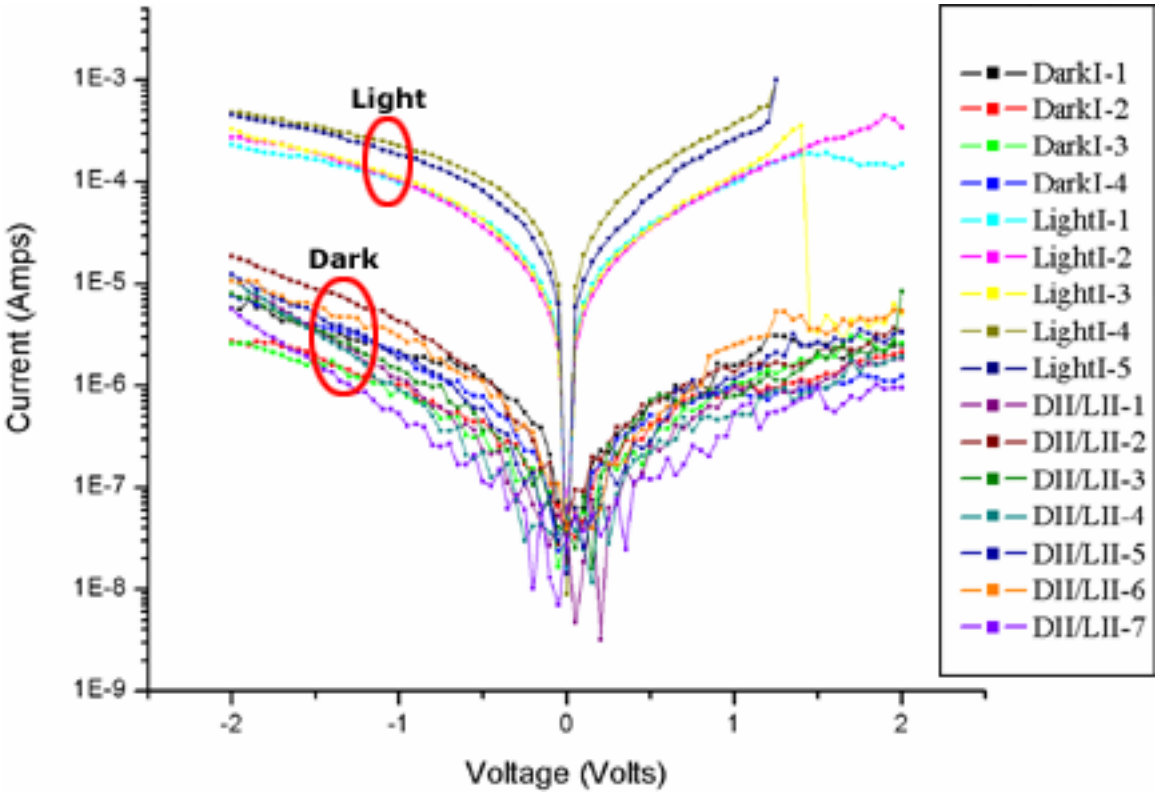

Figure 40: Logarithmic representation of the absolute value of the data from Figure 39.

Since PSI and chlorophyll have very similar absorption spectra, work must be done to determine which is responsible for the device characteristics. One way to do this is to denature the protein and then measure the device's *I-V* characteristic. Figure 41 shows a device prepared just like the device in Figure 39, except that the device was baked for an hour at 150°C. Each plot corresponds to a measurement taken and the legend shows the order in which the measurements were taken. This device exhibits no photocurrent excitation. Many devices on a slide were measured and none generated any photocurrent. Figure 41 resembles a typical example of a device on the slide. The spike at the positive bias for run 9 is a transient of unknown origin.

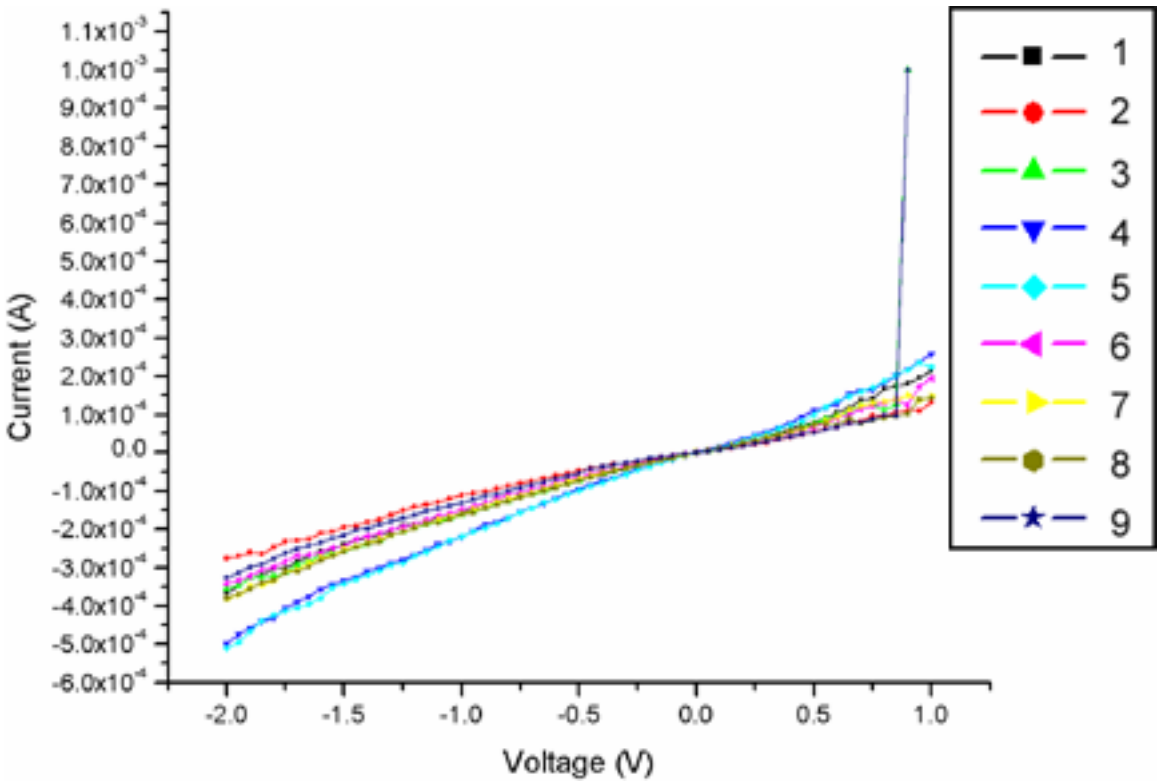

Figure 41: This is the typical response found on an Alq_3 device with a preparation similar to the one in Figure 39 except that it has been baked in an oven at 150°C for one hour. Some shown values were taken in 670nm laser light and others were taken in the dark. Note the large range of values for the current which is similar to the range found in a functional sample of PSI/Alq_3 device in the dark. The numbers of the plots reflect the order in which they were taken.

In addition to Alq_3 devices, CuPc devices were made. These devices were made by letting the gold-covered slide sit for 20 minutes in 200µL of 6mg DTSSP/mL H_2O. Then the slide was soaked in 100µL of 30mg NTA ligand/mL H_2O for 10 minutes. Next, the device was soaked in 4mg glycine quenching buffer/mL H_2O for 15 minutes. Then it was soaked in charging buffer for 10 minutes and then binding buffer for 10 minutes. The device was then placed in a solution containing genetically modified PsaD with a 6 x His tag for 30 minutes. Finally, the device was placed in a solution containing PSI and glucose. The device was then gently dried and allowed to evaporate. When the device was measured with the lock-in monochromator setup with varying biases, the plots in Figure 42 and Figure 43 were obtained. The device characteristic changes with the bias,

but it is difficult to tell whether the device response is due in part to PSI. There is a slight peak near 690nm, but this is due to CuPc's own absorption spectrum. There is no evidence of activity near 670nm, where the PSI is excited. The devices were allowed to sit out for about 24 hours after being made, and the PSI might have denatured on its own by then.

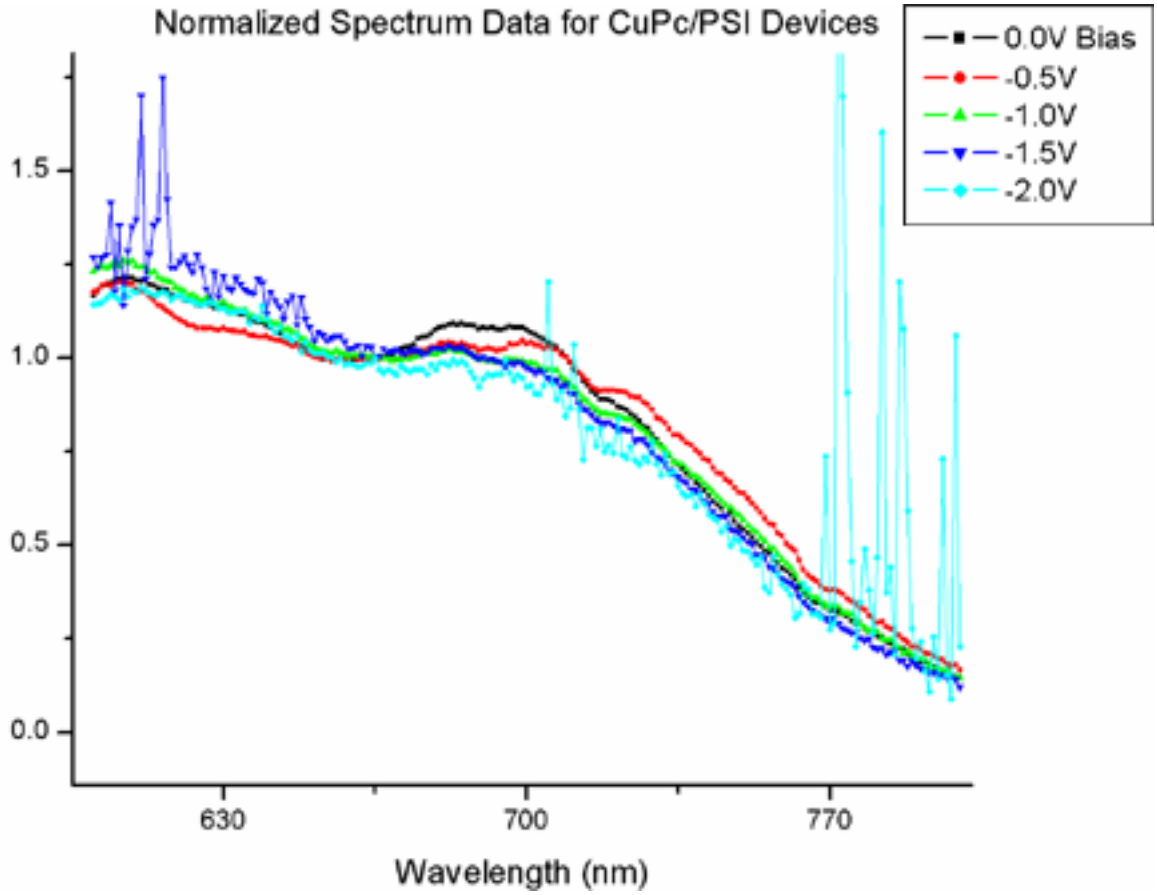

Figure 42: Normalized spectrum data for a voltage biased CuPc/PSI device. This shows the full range from 600nm to 800nm.

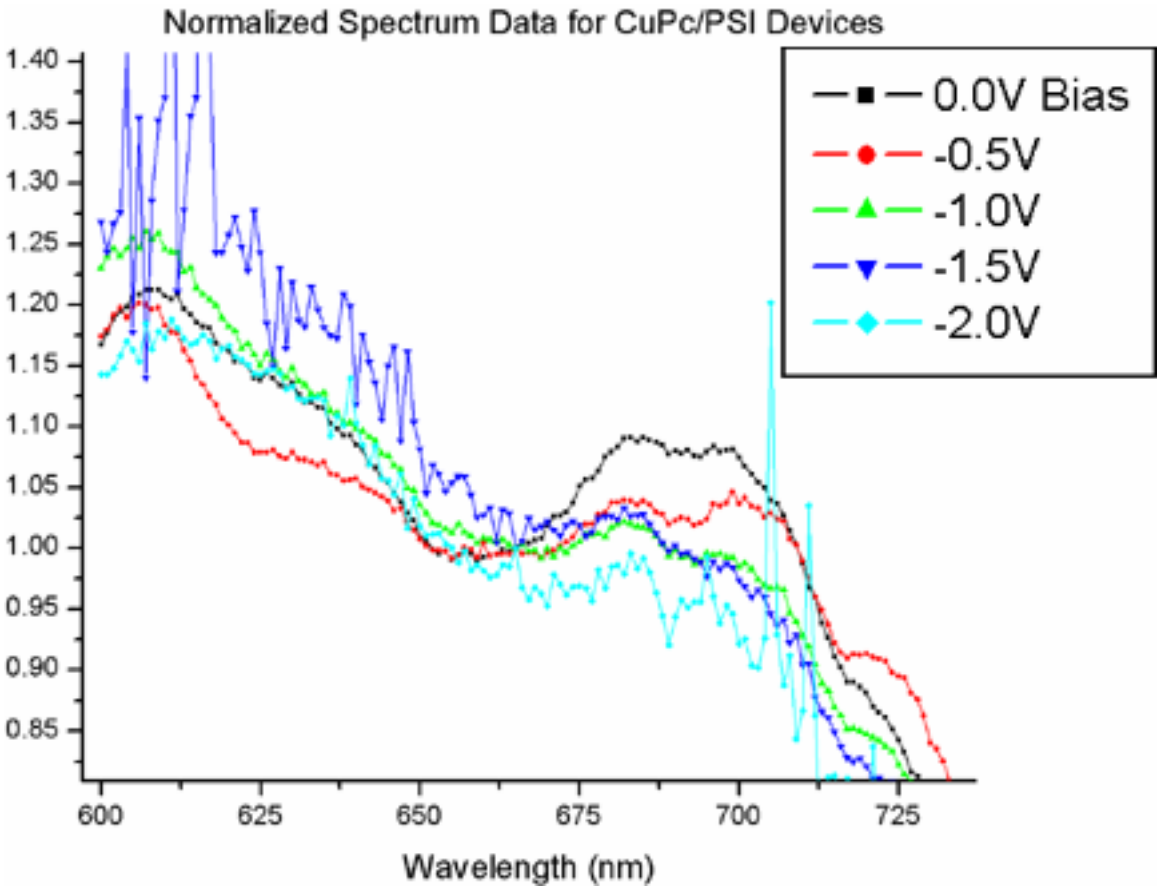

Figure 43: Normalized spectrum data for a voltage biased CuPc/PSI device. This focuses more on the behavior near 670nm.

iii. Solution Processed Device Data

Another method of affixing a protective layer involves solution processing. In solution processing, a protective layer is either spun on or placed in solution form onto a slide and allowed to dry. Two materials have been used for solution processing: polythiophene, a spun on film, and polyvinyl alcohol (PVA) a dried film (Figure 44).

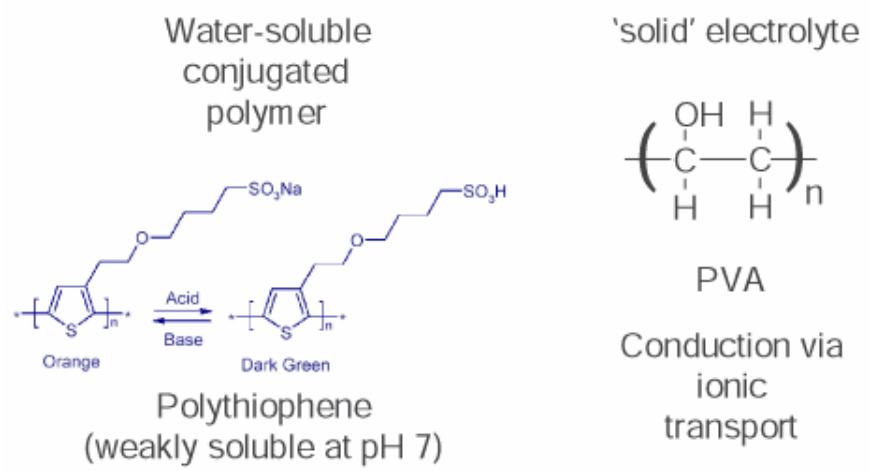

Figure 44: Some materials used in the organic protective layer of PSI devices. Copper phthalocyanine (CuPc) is evaporated onto the device while polythiophene is spun onto the device and polyvinyl alcohol (PVA) is dried onto the device.

Polythiophene, a sulfur-containing polymer, has been known to lock in moisture which is key for preserving PSI as it normally functions in an aqueous environment. However, in order to evaporate on silver contacts, the spun-on film must be able to stay on the device and not vaporize while in vacuum. Therefore, several six slides containing polythiophene were prepared: half coated with polythiophene prepared at room temperature and half prepared with polythiophene heated to 75ºC. One slide from each set was either left in a vacuum environment for 47 cycles between vacuum and atmosphere over the course of 120 minutes, in an oven under vacuum at 100ºC for 120 minutes, or out in atmosphere at room temperature for 120 minutes. The response of each slide was then measured on a spectrophotometer (Figure 45). The sample left unheated showed the greatest response, indicating it retained the most moisture. The heated polythiophene sample kept in the vacuum had the least response, indicating it retained the least amount of moisture. This is because the polymer chains are separated by solvent, decreasing non-radiative losses associated with aggregation. The samples kept in the oven had similar responses. The heated sample in the vacuum may have had

the smallest response due to the air currents introduced while the vacuum chamber was being cycled between vacuum and nitrogen gas. These results show that the polythiophene most likely locks in enough moisture to sustain PSI while it is in solid state.

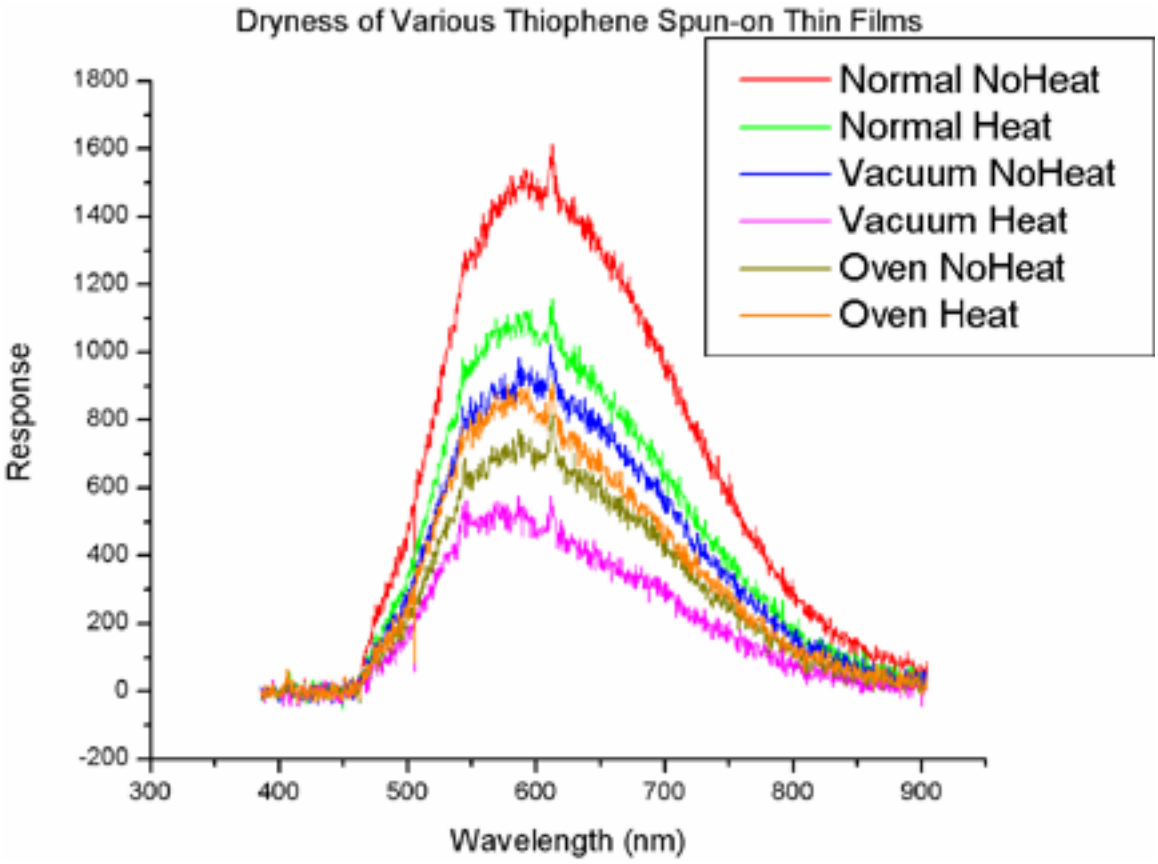

Figure 45: Responses of various samples of polythiophene as measured by a spectrophotometer. A high peak in response indicates more moisture is retained by the sample.

Initial polythiophene devices did not show much promise. However, after several experiments, some devices showed a photo-response, like the one with unoriented PSI in Figure 46. The measurements taken in the presence of 670nm laser light show a jump in photocurrent near 0.5V whereas the measurements taken in the dark show a jump near 1.1V. The PSI, when excited, appears to prevent carrier trapping at the interface, suggesting that the cofactors P700 and Fe_4S_4 act as charge traps.

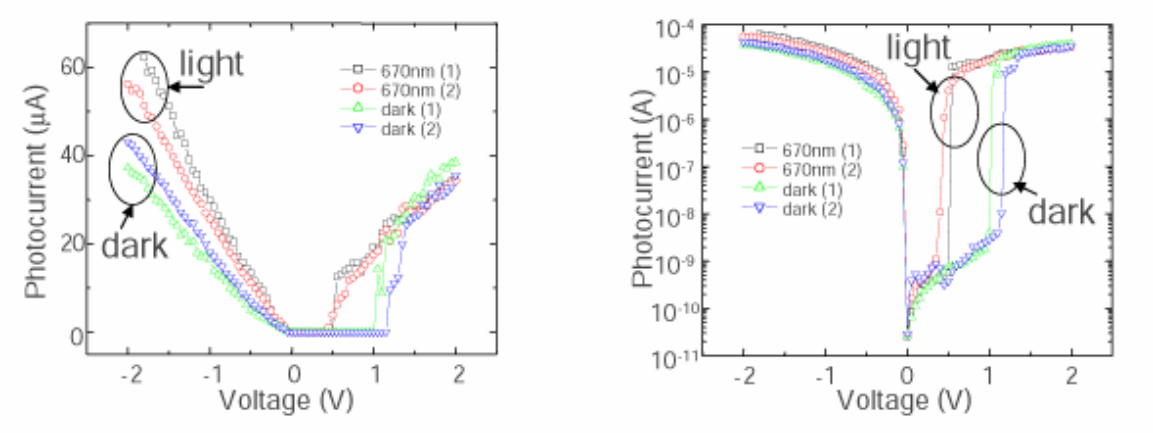

Figure 46: Polythiophene photocurrent. The photocurrent is significantly larger than expected. Here, 2 μW corresponds to 1 mA at 100% quantum efficiency. Optical excitation of PSI appears to prevent carrier trapping at interface, suggesting that P700 and Fe_4S_4 sites act as charge traps. (Data courtesy of Julie Norville)

Devices were also created by drying solubilized PVA and PSI onto an ITO substrate. Devices created using PVA gave different responses for light measurements and dark measurements. However, it appears that some charging within the device takes place as the dark measurement taken immediately after the first light measurement shows an elevated response. It also appears that this charging destroys the system as the second light measurement is similar to the initial dark measurement (Figure 47).

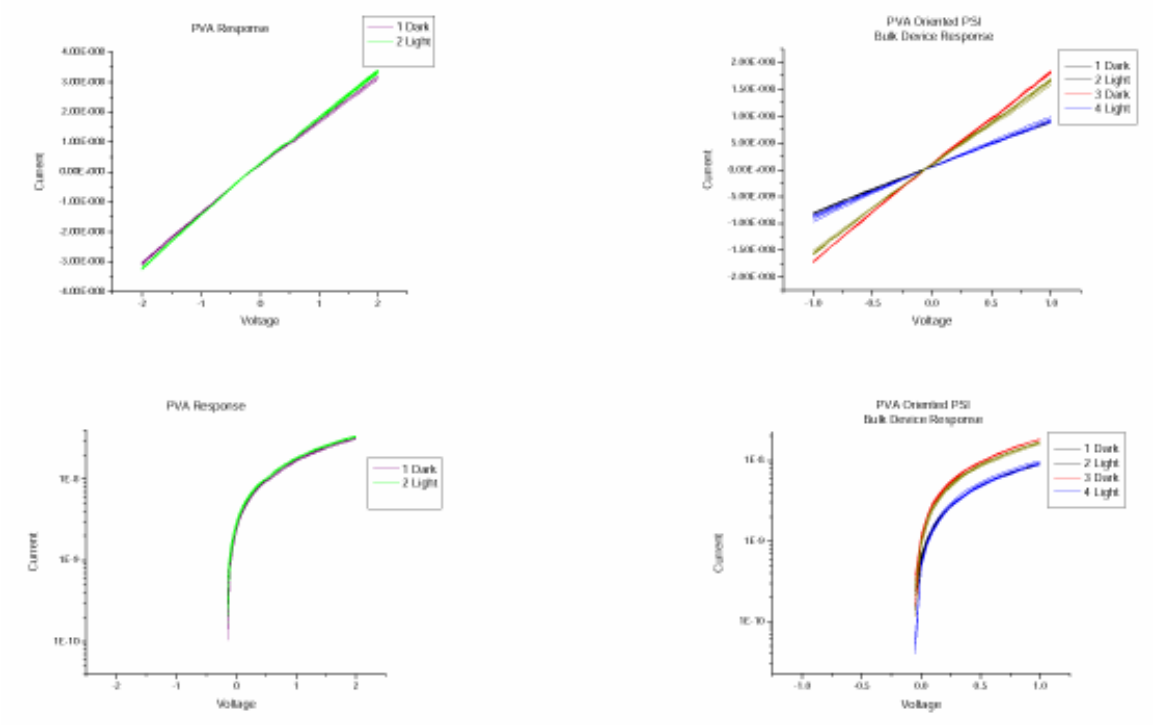

Figure 47: *I-V* response of PVA (left) on linear and logarithmic axes and PVA-oriented PSI bulk device response (right) on linear and logarithmic axes. Note the two different sets of graphs in the right two pictures. The "red group" consists of a light and dark sample as does the "blue group." Measurements were taken first in the dark, then in the light, then in the dark again and then in the light the dark. (data courtesy of Julie Norville)

Solution processed devices tend to fare better than evaporation processed devices. This could be due to the exposure to vacuum that is unavoidable due to the nature of evaporation processing. It could also be true that the solution processed layers protect the PSI better than evaporated layers.

V. Conclusion

Devices containing photosynthetic reaction centers show great promise as photodetectors. These experiments show that PSI continues functioning while in solid state devices.

The measured devices give evidence that PSI is oriented on a substrate. Atomic force microscopy images show the formation of oriented trimers of PSI. Absorption spectra taken of the protein in the device reveal the characteristic absorption for PSI. These show that PSI may still function while bound to the gold substrate. Although it remains difficult to distinguish between intact PSI and chlorophyll spectroscopically, this is not a problem with bacterial RC's. The reaction centers might be a better candidate for devices since they have a more structured spectrum, making it easier to distinguish between this protein and chlorophyll.

More AFM images should be made, especially for voltage sensitive images. There are minute deviations which occur in repeated scans of samples which might partially account for the different behavior seen with different tip voltages. In all likelihood, the applied voltage is causing the changes.

There is some evidence supporting the theory that PSI unreliably functions while in the final device complete with cathodes and an organic protective layer. Curves taken with an HP4156 analyzer show *I-V* curves which indicate photo-sensitive behavior. However, devices measured using the lock-in monochromator setup did not show strong evidence for PSI. This could be due to the relatively low intensity of light in this setup as compared with the laser setup. There is no strong evidence indicating whether the chlorophyll molecules in PSI are responsible for the device behavior or whether the PSI

is intact. More *I-V* characteristics of baked PSI devices would show demonstrate what of the two is responsible for the behavior seen. HP4156 scans of baked devices should be repeated with better controls that have a high density of working photosensitive devices.

To make longer lasting devices, much more work must be conducted in order to remedy the current problems with these preliminary devices. One potential source of problems is the evaporation process. Subjection of the device to vacuum conditions may cause damage to the delicate biomolecular complexes. A possible alternative is to use lamination, a method wherein contacts can be created without thermal evaporation. However, there is no data either way which definitively implies that thermal evaporation is harmful.

Preparation of the complexes also leads to different results. More research must be conducted into which third parties supply the best quality product. Certain batches of protein may work better in solid state devices than others. This is due to the complex steps necessary to extract pure PSI from plant cells. In-house production may allow for direct binding to the substrate from a solution of plant cells using the method described by Goldsmith and Boxer.

In the future, it will be important to create devices which last longer. Currently, devices stop functioning after one photo-excitation. This could be due to the high intensity of the laser. Trying measurements with a laser of lower power or a laser tuned to the frequency of a smaller absorption peak will help determine if any harm is caused by the laser. Additionally, PSI and bacterial RCs require transport molecules to carry away excess charge developed in their reaction core during photosynthesis. This molecule is absent in our current experiments. Adding this transport chemical, ferredoxin,

might help devices last longer. Another possible solution is to use a Langmuir-Blodgett film of an entire thylakoid membrane. Since photosynthesis is a process that occurs in the thylakoid membrane, keeping the protein in a state resembling its natural environment may make it last longer.

Photovoltaic cells could be created in the future by altering the substrate. By creating a very rough substrate and coating it with a high density of biocomplexes, it is possible to obtain a photovoltaic device. Creating such a device will demonstrate the viability of the complexes.

In general, more work must be done in regard to determining optimal parameters for spin-coating and evaporation. The materials play a great role in the device and now that some materials have been determined to be better than others (i.e. Alq_3 generally gives better results than CuPc), the next step should be to determine how to optimize the activity of these materials. Also, more work should be conducted into the effect of a vacuum environment on the materials used as the organic protective layer.

Due to the precise nature of the biocomplexes, they are optimized for giving rise to excitons when excited by light. This gives the devices enormous potential for use as photodetectors and photovoltaics.

VI. Appendix

A. LabVIEW Program

i. Lockin-Monochromator_SimultaneousCalibration_PostOpDivide_RawData.vi

---

Connector Pane

Front Panel

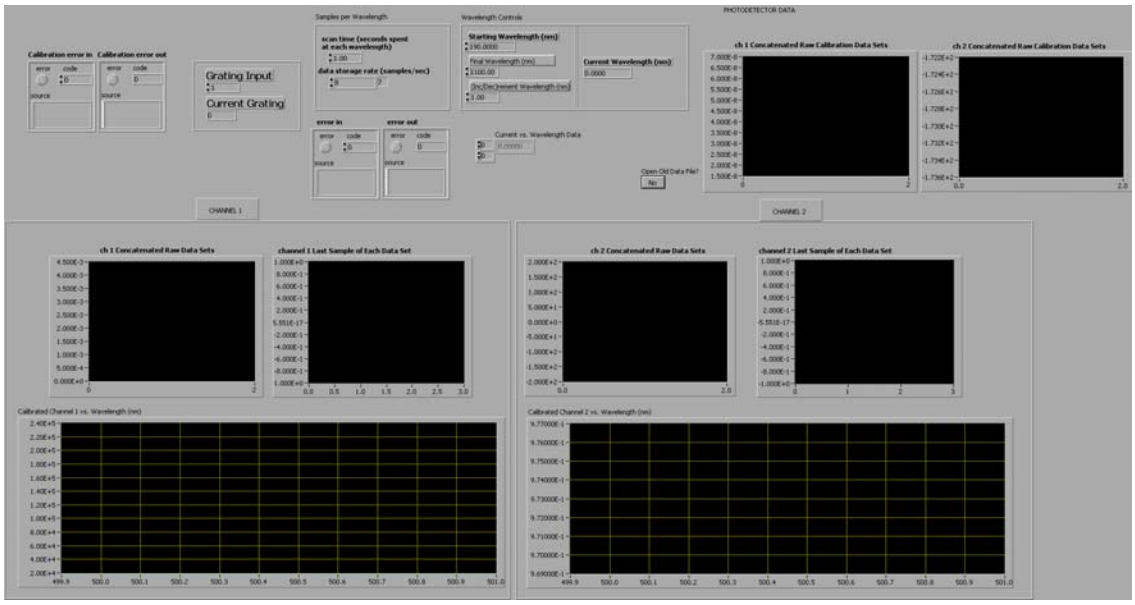

Controls and Indicators

error in
- error
- code

source

scan time (seconds spent at each wavelength)

The scan length is the approximate length of the data acquisition scan in seconds .

data storage rate (samples/sec)

The sample rate sets how often points are added to the storage buffers .

Range : 0.0625 Hz to 512 Hz

Starting Wavelength (nm)

(Inc/Dec)rement Wavelength (nm)

Final Wavelength (nm)

Open Old Data File?

Calibration error in

- **error**
- **code**
- **source**

Grating Input

ch 1 Concatenated Raw Data Sets

This array contains the channel 1 points which can be connected to Labview analysis VIs .

error out

- **error**
- **code**
- **source**

channel 1 Last Sample of Each Data Set

Current Wavelength (nm)

Calibrated Channel 1 vs. Wavelength (nm)

Current vs. Wavelength Data

ch 2 Concatenated Raw Data Sets

This array contains the channel 2 points and can be connected to Labview analysis VIs.

channel 2 Last Sample of Each Data Set

Calibrated Channel 2 vs. Wavelength (nm)

Calibration error out

error

code

source

ch 2 Concatenated Raw Calibration Data Sets

This array contains the channel 2 points and can be connected to Labview analysis VIs.

ch 1 Concatenated Raw Calibration Data Sets

This array contains the channel 1 points which can be connected to Labview analysis VIs .

RAW Current vs. Wavelength Data

Current Grating

Block Diagram

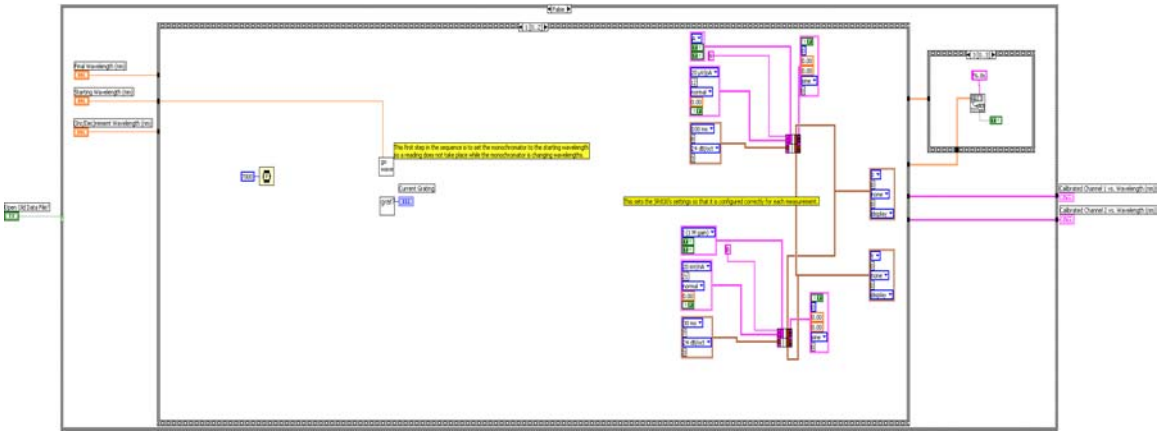

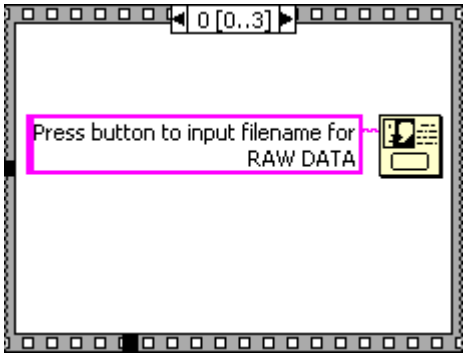

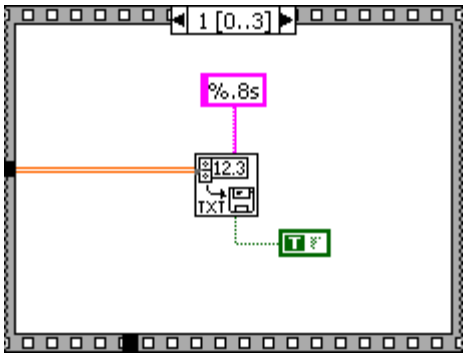
1 [0..3]
%.8s
12.3
TXT

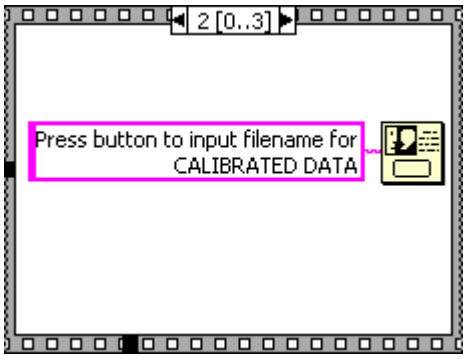
2 [0..3]
Press button to input filename for
CALIBRATED DATA

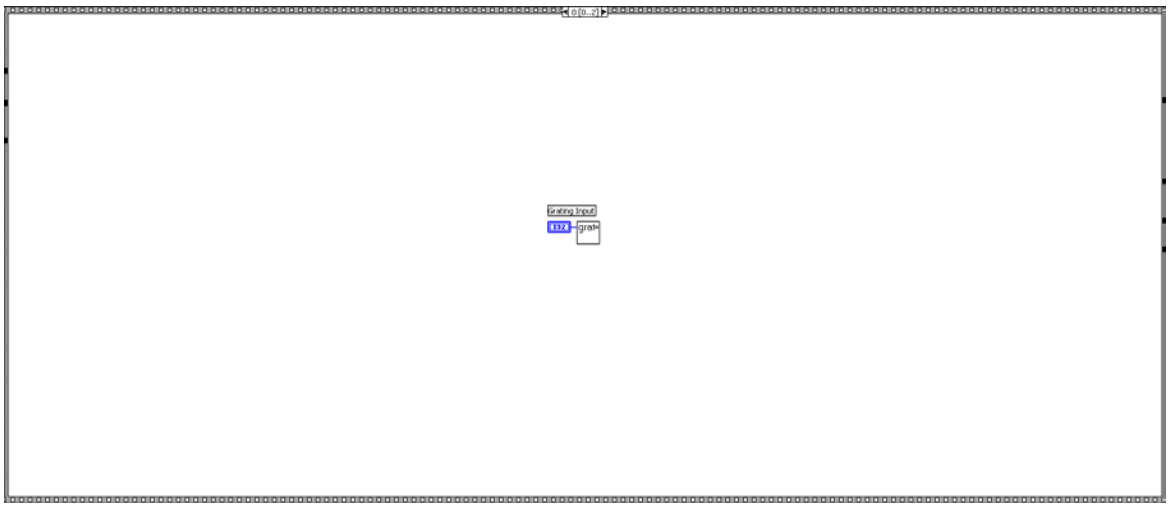

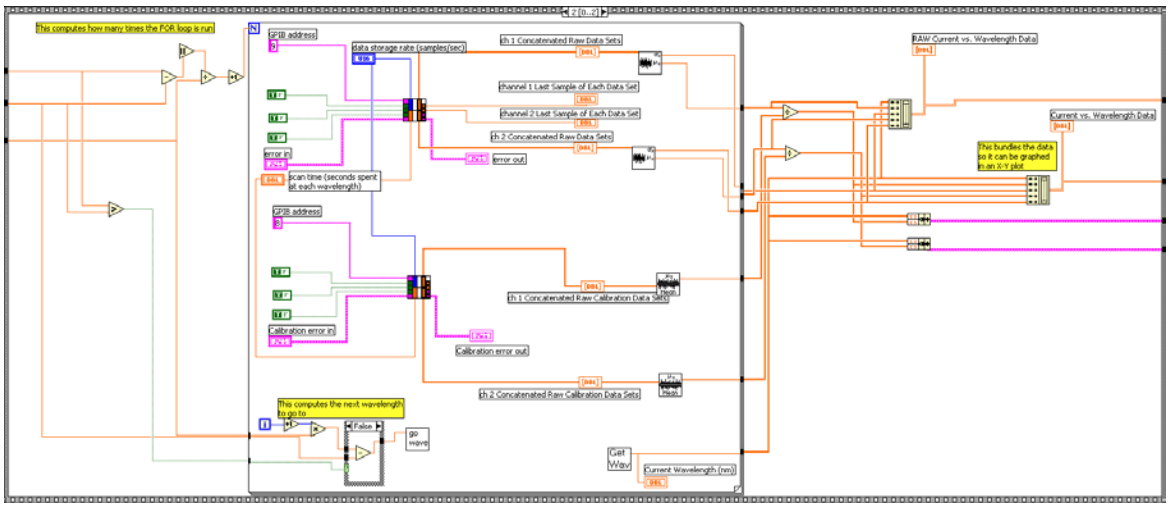

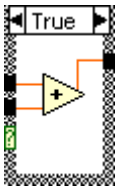

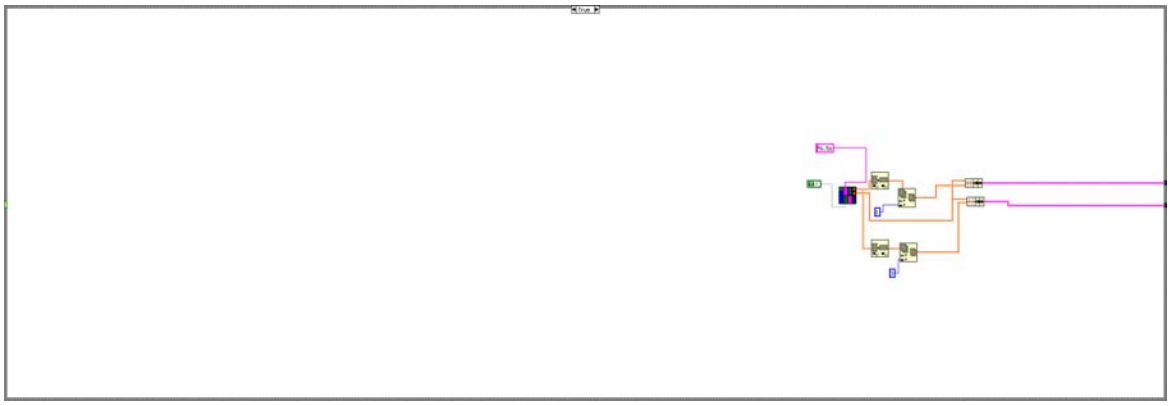

List of SubVIs

SR830 DATA STORAGE EXAMPLE.VI

C:\Program Files\National Instruments\LabVIEW\instr.lib\sr830\SR830.LLB\SR830 DATA STORAGE EXAMPLE.VI

GetWave.vi

C:\Program Files\National Instruments\LabVIEW\instr.lib\cornerstone130\GetWave.vi

gowave.vi

C:\Program Files\National Instruments\LabVIEW\instr.lib\cornerstone130\gowave.vi

Read From Spreadsheet File.vi

C:\Program Files\National Instruments\LabVIEW\vi.lib\Utility\file.llb\Read From Spreadsheet File.vi

SR830.VI

C:\Program Files\National Instruments\LabVIEW\instr.lib\sr830\SR830.LLB\SR830.VI

Standard Deviation.vi

C:\Program Files\National Instruments\LabVIEW\vi.lib\Analysis\5stat.llb\Standard Deviation.vi

Mean.vi

C:\Program Files\National Instruments\LabVIEW\vi.lib\Analysis\5stat.llb\Mean.vi

Write To Spreadsheet File.vi

C:\Program Files\National Instruments\LabVIEW\vi.lib\Utility\file.llb\Write To Spreadsheet File.vi

setgrat.vi

C:\Program Files\National Instruments\LabVIEW\instr.lib\cornerstone130\setgrat.vi

getgrat.vi

C:\Program Files\National Instruments\LabVIEW\instr.lib\cornerstone130\getgrat.vi

---

History

"Lockin-Monochromator_SimultaneousCalibration_PostOpDivide_RawData.vi History"

Current Revision: 151

ii. Standard Operating Procedure

SOP for lock-in/Monochromator program

Revision: 1.6

Author: Rajay Kumar

Revision History:

05/03/2003: 1.6 – Rajay Kumar, included instructions on how to set lock-in parameters before measurement runs.

04/29/2003: 1.5 – Rajay Kumar, included new changes specified at the end of the file to include for simultaneous calibration, saving of raw data, multiple channels.

10/24/2002: 1.4 – Rajay Kumar, updated file to include specifications for naming files and to describe how to change bias settings.

10/22/2002: 1.3 – Rajay Kumar, updated to include all inputs which should be recorded and also new function of recording standard deviations in the saved files.

10/17/2002: 1.2 – Rajay Kumar, updated to include ability to run program backward (start at high wavelength and decrement to smaller wavelength). Made minor typographical changes.

9/23/2002: 1.1 – Rajay Kumar, updated to include changes to program and to clarify setup.

8/2002: 1.0 – Rajay Kumar, original SOP

This program coordinates a monochromator to tune to a specific wavelength, make the lock-in amplifiers take some readings for that wavelength and then change the wavelength and take more readings. One lock-in measures values taken directly from the device. The other lock-in measures values taken from a Newport photodetector intercepting light from the monochromator split by a beamsplitter. These values are used to calibrate the data by dividing the raw data by the calibrated data at the end of the program's run.

This program's final output, "averages vs. wavelength," shows the calibrated data. Since the averages vs. wavelength is only shown after the experiment is run, I have included some semi-useful real-time graphs:

When running the program, the user should set the monochromator to a setting where the device will give off a large photocurrent or photovoltaic response. Then, adjust the lock-in settings to their optimal values. Then go to the diagram of the program and go to the sequence pane 1 when the outermost box is set to false. In here are diagrams for both lock-ins. One corresponds to a lock-in with a GPIB address of 8 and the other corresponds to a lock-in with a GPIB address of 9. The lock-in at address 8 is for the photodetector calibration while 9 is for the device. Input the optimal values for each lock-in: time constant, sensitivity, channel displays, etc. After this, the user can run the

program when the desired values for the front panel are inputted. If the user is just opening a file, changing the values in the diagram is unnecessary.

Concatenated Raw Data Sets:
This shows the raw data that the program is receiving. For each wavelength, it will record (scan length * data storage rate) values. E.g., if scan length is 2.00 and data storage rate is 4, then for each wavelength, this graph will show 2.00 * 4 = 8 points. This graph is a "moving window." That is, it will show only a set number of points (about 1000) and therefore show only one section of the data at once. This is shown for channels 1 and 2 for one lock-in as well as for channels 1 and 2 for the calibration lock-in.

Last Sample of Each Data Set:
This shows the last sample of each of the (scan length * data storage rate) points. The vast majority of the time, this will be close to the mean and will closely resemble the final graph if you graph enough points. It also shows all graphed points at once. This is shown for Channels 1 and 2 of only one the raw-data collecting lock-in.

The Current vs. Wavelength graph will remain empty until the program finishes. When the program is done, prompts will appear, letting you save the data. The first prompt lets the user save raw data and the second lets the user save calibrated data. The data will be in 5 tab-separated columns with wavelength in the first column, channel 1 in the second, the standard deviation of channel 1 in the third column, channel 2 in the fourth column, and the standard deviation of channel 2 in the fifth column. I recommend saving the calibrated file as a text (.TXT) file. The naming convention I have adopted is of this form: NAME_*{starting wavelength}_{final wavelength}*!*{increment_or_decrement}_{notes}*.txt. The *{notes}* can be used to write any distinguishing characteristics, like "CAL" if the data used a calibration file. If I measured an ALQ device, going backwards from 700nm to 400nm with a bias of 1V, a gain of 1E06 V/A, a lamp power of 220W and used a calibration file, I would call it "ALQ_700_400!1_BIAS1V_GAIN1E06_POWER220W_CAL.txt". (Windows 2000 can handle file names of at most 256 characters). I recommend saving the raw data in a similar way, but with the addition of the word "RAW" at the end of the filename.

INPUTS:
Scan length: The time in seconds you want the lock-in to spend at each data point. This is also the time the monochromator will spend at each wavelength. One or two seconds should be fine.

Data storage rate: This is in units of samples per second. Multiply this by the scan length and you have the number of samples you are taking per wavelength. A larger product will mean more precise results, but longer computation.

Starting Wavelength: This is the wavelength at which the monochromator should start its scan at. It is in nanometers. Since calibration data is provided for wavelengths as low as 190nm, the starting wavelength should not be lower than this. If the wavelength is below the system's bottom threshold, the program will stop, according to its manual.

Final Wavelength: This is the wavelength at which the monochromator should end its scan. It is in nanometers. Since calibration data is provided for wavelengths as high as 1100nm, the final wavelength should not be higher than this. If the wavelength is higher than the system's upper threshold, the program will stop, according to its manual.

Increment Wavelength: This is how many wavelengths the scan should increment itself by before taking another measurement. This must be less than the Final Wavelength minus the Starting Wavelength. If it is not, unknown behavior will occur. It must also be greater than zero (the default value).

Open 2 Column Data File: Changing this button to "YES" and then running the program will make the program open a file and show it in the graph.

Grating Input: There are 2 gratings in the Cornerstone monochromator which have different responses to the input light. One grating may have greater power for certain wavelength over another grating. Grating 2, for example, has twice the output current when the wavelength is at 800nm as measured by the Newport photodetector.

Calibration Error In and Error In: Do not use these inputs. These are for testing only.

Miscellaneous Inputs: These are inputs from physical laboratory equipment. You can change the gain and bias on the Keithley 428 Current Amplifier to your specifications. Higher gains can give the lockin more stability. These values should be recorded manually or input directly as part of the name of your file. Another thing you can adjust is the ouput power of the lamp. This will generally be between 100W and 220W (it can go higher, but has a hard time remaining steady at the higher values).

To set the gain on the Current Amplifier, Make sure the GAIN LED is high-lighted on the SETUP interface and then use the ADJUST knob to change values. To use a bias, first make sure the VOLTAGE BIAS LED is on under the ENABLE interface. Then press VOLTAGE BIAS on the SETUP interface and use the ADJUST knob to change the value.

OUTPUTS:
Current Wavelength: This is the wavelength to which the monochromator is currently set.

Current vs. Wavelength Data: This lets the user check what data is stored at a certain point. If the higher value is 0, then the lower value will select wavelengths. If the higher value is 1, then the lower value will select current.

Calibration Error Out and Error Out: If the program stops unexpectedly, the error "light" will be black and a text message will be displayed in "source." To proceed with another scan, the error light must be clicked using the "operate value" (pointing finger) cursor and turned off. Most of the time, the light should be off.

Current Grating: This shows which grating is currently selected: either grating 1 or grating 2.

The output files will now include columns which record the standard deviation of recorded data. These will be found in the 3rd and 5th columns of the output files for channels 1 and 2, respectively.

Required Equipment:
(All must be on in order to use program properly)

- Two SR830 Lock-in Amplifiers (Switch is in back, near bottom)
- Oriel Lamp (NOTE: After turning on box, press Lamp On button)
- Cornerstone Monochromator
- Keithley 428 Current Amplifier (NOTE: After turning on, press Zero Check button so indicator LED is off)
- Chopper (set behind the output of the monochromator)
- Beam splitter (usually set just behind the chopper)j
- Newport 818-UV photodetector (set to intercept light reflected by the beamsplitter)

(make sure all are off when done experimenting so we don't burn out bulbs/wear out motors)

Known bugs/issues:

- Graphs must be cleared before proceeding with another scan. Otherwise, new data will be concatenated onto old data (file data will be fine though). To clear graph data, right-click on the graph, click on "Data Operations" and then click on "Clear Graph"
- To see the data in Origin, simply click on "Import Ascii" and open the text file. It will then be in tabular form
- Pressing the Tab button will change the cursor from a hand with a finger to an arrow. The arrow will not select input spaces; instead it will move around inputs. If any changes are made to the program layout, simply quit the program, say "No to All" when prompted to save and re-open the program.
- The user must use the diagram to change settings such that the lock-in works properly for each run.

Recent fixes/additions:

- Moved the program from a Windows XP system to a Windows 2000 system. This eliminated the frequent crashes and random "zeroing" of data.
- Inserted code to set the lock-in to the proper parameters at the start of each scan. I also had to change the pause in the beginning of the program from 5 seconds to 7 seconds in order to give the lock-in time to adjust from any overload readings it may have had before.
- Included an option to open just a graph.
- Included an option to divide final data by a calibration dataset.

- The program can be run backward now, starting at a wavelength higher than the final wavelength. This is useful for devices where early excitations from higher wavelength light can be detrimental to device function.
- Added graphs showing both channels
- Included functionality to do simultaneous calibration with a photodetector where the data is divided at the end.
- Added a feature allowing the saving of raw data.

B. References

1. Biology Project, The. Photosynthesis Problem Set 1: Problem 7 Tutorial: Cyclic photophosphorylation. *The Biology Project.* (1996) < http://www.biology.arizona.edu/biochemistry/problem_sets/photosynthesis_1/07t.html>

2. Bulović, V. Growing and Pattering Thin Organic Films I. *6.973 Class Lecture Notes.* (2003) <http://stellar.mit.edu/S/course/6/sp03/6.973/courseMaterial/topics/topic7/lectureNotes/L12/L12.pdf>

3. Campbell, M. Amino Acid Abbreviations. *Molecular Biology (Bio304).* (2002) < http://www.bio.davidson.edu/courses/Molbio/aatable.html>

4. Frydrych, M., Lensu, L., Aschi, C., Parkkinen, S., Parkkinen, J., Jaaskelainen, T. Model of Photovoltage Response of Bacteriorhodopsin in PVA Films. *Computational Nanoscience 2001.* ISBN 0-9708275-3-9. (2001). <www.cr.org>.

5. Energy Information Administration (EIA). *Renewable Energy Annual 2001.* (2001) <http://www.eia.doe.gov/cneaf/solar.renewables/page/rea_data/preface.html>

6. Goldsmith, J.O., Boxer, S.G. Rapid isolation of bacterial photosynthetic reaction centers with an engineered poly-His tag. *Biochimica et Biophysica Acta.* **1276** (1996) 171-175.

7. Greenbaum, E. Platinized Chloroplasts: A Novel Photocatalytic Material. *Science.* **230**, (1985) 1373-1375.

8. Hallick, R. Chloroplasts. *Biology 181.* (2001) <http://www.blc.arizona.edu/courses/181gh/rick/photosynthesis/chloroplasts.html>

9. Kaiser, G. Noncyclic Photophosphorylation. *BIOL 230.* (2001) < http://www.cat.cc.md.us/courses/bio141/lecguide/unit1/eustruct/phofig2.html>

10. Katz, E. Application of bifunctional reagents for immobilization of proteins on a carbon electrode surface: oriented immobilization of photosynthetic reaction centers. *Journal of Electroanalytical Chemistry.* **365** (1993)157-164.

11. Lee, I., Lee, J. W., Greenbaum, E. Biomolecular Electronics: Vectorial Arrays of Photosynthetic Reaction Centers. *Physical Review Letters.* **79,** (1997) 3294-3297.

12. Lee, I., Lee J. W., Stubna, A., Greenbaum, E. Measurement of Electrostatic Potentials above Oriented Single Photosynthetic Reaction Centers. *Journal of Physical Chemistry B.* **104** (2000) 2439-2443.

13. Madigan, C. Thermal Evaporator: Standard Operating Procedures.

14. Minai, L., Fish, A., Darash-Yahana, M., Verchovsky, L., Nechushtai, R. The Assembly of the PsaD Subunit into the Membranal Photosystem I Complex Occurs via an Exchange Mechanism. *Biochemistry.* **40** (2001) 12754-12760.

15. National Center for Biotechnology Information (NCBI). Molecular Modeling Database (MMDB). Crystal Structure Of Photosystem I: A Photosynthetic Reaction Center And Core Antenna System From Cyanobacteria. <http://www.ncbi.nlm.nih.gov/Structure/mmdb/mmdbsrv.cgi?form=6&db=t&Dopt=s&uid=16884>.

16. Peumans, P., Forrest, S. R. Very-high-efficiency double-heterostructure copper phthalocyanine/C_{60} photovoltaic cells. *Applied Physics Letters.* **79** (2001) 126-128.

17. Peumans, P., Bulović, V., Forrest, S. R. Efficient, high-bandwidth organic multilayer photodetectors. *Applied Physics Letters.* **76** (2000) 3855-3857.

18. Purves, Orians, Heller. *Life: The Science of Biology, Fourth Edition*. Sinauer Associates, Inc. Sunderland, MA. (1995) 162-187.

19. Richardson, R. Photosynthesis. *Biology 201.* (2002) < http://scidiv.bcc.ctc.edu/rkr/Biology201/lectures/Photosynthesis/Photosynthesis.html>

20. Robertson, B., Lukashev, E.P. Rapid pH change due to bacteriorhodopsin measured with a tin-oxide electrode. *Biophysical Journal.* **68** (1995) 1507-1517.

21. Schubert, W.-D., Klukas, O., Krauß, N., Saenger, W., Fromme, P. & Witt, H. T. Photosystem I of Synechoccus elongates at 4Å Resolution: Comprehensive Structural Analysis. *J. Mol. Biol.* **272** (1997) 741-769.

22. Smith, H. *Submicron- and Nanometer-Structures Technology.* 2nd Edition. (1994) 8-12 – 8-15.

23. Stanford Research Systems, Inc. MODEL SR830 DSP Lock-In Amplifier (manual). Revision 2.0. (2002). <ftp://ftp.thinksrs.com/PDFs/Manuals/SR830m.pdf>